Physics – Uspekhi **59** (4) 367 – 382 (2016)

60th ANNIVERSARY OF THE JOINT INSTITUTE FOR NUCLEAR RESEARCH (JINR) PACS numbers: **12.38. – t**, **12.39. – x**, 25.75.Nq

Phase diagram of baryon matter in the SU(2) Nambu – Jona-Lasinio model with a Polyakov loop

Yu L Kalinovsky, V D Toneev, A V Friesen

DOI: 10.3367/UFNe.0186.201604b.0387

Contents

Abstract. The nature of phase transitions in hot and dense nuclear matter is discussed in the framework of the effective SU(2) Nambu – Jona-Lasinio model with a Polyakov loop with two quark flavors — one of a few models describing the properties of both chiral and confinement–deconfinement phase transitions. We consider the parameters of the model and examine additional interactions that influence the structure of the phase diagram and the positions of critical points in it. The effect of meson correlations on the thermodynamic properties of the quark–meson system is examined. The evolution of the model with changes in the understanding of the phase diagram structure is discussed.

Keywords: phase diagram, phase transition, spontaneous chiral symmetry breaking, confinement, critical end point, thermodynamics of quark matter, meson correlations

1. Introduction

The properties of nuclear matter under extremely high pressures and temperatures have been studied in many theoretical papers and can be explored in new accelerators and experiments capable of reproducing these conditions. Special attention in given to searches for the phase transition from hot dense matter to the quark–gluon plasma. In hot and dense nuclear matter, after nucleon overlapping, a state can arise where quarks cannot be uniquely assigned to a given object. Such a system can be regarded as a gas of quasi-free particles consisting of strongly interacting quarks and gluons (the quark–gluon plasma).

Presently, quantum chromodynamics (QCD) is the commonly accepted theory of strong interactions, in which the interaction between quarks and gluons is mediated by color exchange [1]. The non-Abelian nature of QCD enables introducing and describing two basic QCD features: asymptotic freedom and confinement. Asymptotic freedom is the ability of a QCD system to weakly interact at high energies. Confinement is the ability of quarks to form colorless states (hadrons) in normal conditions (low temperatures and densities). It is difficult to use the QCD Lagrangian to directly calculate the mass spectrum, coupling constants, and physical processes in nuclear matter. To investigate phase states of nuclear matter, direct lattice QCD calculations [2] have been used. Phase transitions in hot and dense nuclear matter suggest that with increasing the temperature and/or density, deconfinement (liberation of quarks) can occur, and the mass of quarks is reduced to its current value. To fully describe the phase diagram structure, a theory embodying the basic principles of quark–gluon interactions is needed.

The lattice QCD suggests that a chiral phase transition (partial chiral symmetry restoration due to conversion of massive quarks into current quarks) occurs at the temperature $T_c^{\rm lat} \approx 0.154 \pm 0.009$ GeV [2] in the case of $2+1$ quark flavors and at 0.170 GeV in the case of two flavors [3], and it should coincide with a deconfinement-type transition. The lattice QCD approach may be quite precise, but there are issues related, for example, to the insufficient power of modern computers, which prevents making an elementary cell sufficiently small. In addition, the quark mass used in lattice calculations is an order of magnitude larger than that of real quarks. The lattice calculations also meet difficulties in regions with a finite chemical potential. This is related to the appearance of a complex determinant when integrating over fermionic degrees of freedom. Calculations with two quark flavors are free from the last problem [4].

Yu L Kalinovsky, V D Toneev, A V Friesen
Joint Institute for Nuclear Research,
ul. Joliot-Curie 6, 141980 Dubna, Moscow region, Russian Federation
E-mail: kalinov@nusun.jinr.ru, avfriesen@theor.jinr.ru

Received 13 July 2015, revised 1 December 2015
Uspekhi Fizicheskikh Nauk **186** (4) 387 – 403 (2016)
DOI: 10.3367/UFNr.0186.201604b.0387
Translated by K A Postnov; edited by A M Semikhatov

These complications, in particular, motivated the development of effective QCD models like the Nambu–Jona-Lasinio (NJL) model [5, 6] or the linear σ-model [7] as low-energy limits of QCD. The NJL model was formulated in 1961 [5] in analogy with the Bardeen–Cooper–Schrieffer (BCS) theory of superconductivity, but did not include notions of quarks and gluons. For quarks, the model was reformulated somewhat later in [8, 9], where it was shown how the current quarks with zero mass $m = 0$ (the chiral limit) are transformed into massive quarks with the mass $m \sim 0.3$ GeV that form hadrons via a spontaneous chiral symmetry breaking mechanism. Volkov and co-authors [10–13] proposed a more realistic variant of the model with nonzero masses of current quarks ($m_0 \sim 0.5$ MeV). A great advantage of the NJL model is the possibility of studying the mass and internal properties of mesons at finite temperatures and densities [14–21].

The NJL model includes four-fermion point-like interactions and is therefore nonrenormalizable, and the choice of an appropriate regularization is essential in order to apply this model [17, 20, 22]. The constraints imposed by this choice are relaxed in a nonlocal version of the Nambu–Jona-Lasinio model [23–25]. But the problem of the choice of the nonlocal interaction form emerges. For example, the instanton representation of the QCD vacuum can be used to construct a nonlocal theory [26–28].

The local interaction in the NJL model does not allow describing confinement. But the NJL model remains relevant because the presence of confinement is not essential in many processes. A model coupling quarks to a homogeneous background gauge field whose dynamics is described by a Polyakov loop [29–32] was proposed on the basis of the NJL model in 2004 [33–35]. The Polyakov-loop extended NJL (PNJL) model is widely used to study the thermodynamic properties of hadron matter under critical conditions in heavy-ion collisions [34, 36–38] and in neutron star interiors (see, e.g., [39–41]).

A shortcoming of the PNJL model is that the critical temperature of the phase transition with a nonzero chemical potential is significantly higher (~ 0.23 GeV) than the lattice QCD value (~ 0.17 GeV) or even the usual NJL one (~ 0.19 GeV). In order to decrease the phase transition temperature, the authors of [34, 35] suggested renormalizing the model parameter T that determines the deconfinement temperature in the absence of free quarks, down to $T_0 \sim 0.19$ GeV. Such an approach indeed decreased the temperature T_c, but the chiral phase transition temperature and the deconfinement temperature then became different, again in contradiction to lattice QCD calculations [42], which were carried out with an imaginary quark (μ_q) [43–45] and an imaginary isospin (μ_I) [46, 47] chemical potential and showed that these temperatures coincide within numerical errors. Therefore, there should certainly be a strong coupling between the quark condensate and the gauge field. The author of [48] proposed to enhance the scalar coupling by adding a phenomenological dependence of the four-quark coupling constant on the Polyakov loop field Φ [49–51]. This formulation of the PNJL model indeed decreases the phase transition temperature by renormalizing T_0 from 0.27 to 0.19 GeV, and the phase transition temperatures then coincide [52].

The phase diagram structure is also affected by the inclusion of repulsion between quarks (or a vector coupling). This problem was considered in both the NJL [53, 54] and PNJL [38, 55–60] models. In the QCD phase diagram, the vector coupling decreases the domain of the first-order phase transition, until its complete disappearance when the coupling constant is sufficiently large. The situation changes in the nonlocal NJL model with a Polyakov loop. This model shows that the first-order phase transition region does not depend on the vector coupling strength (see, e.g., [61]). The vector coupling constant dependence on the Polyakov loop field was discussed in [51, 52]. In the obtained model, not only the chiral phase transition coincides with the confinement–deconfinement transition but also the first-order phase transition domain disappears at much larger values of the vector coupling constant.

Most of the papers studying the thermodynamic properties of the quark–hadron system in the framework of the NJL or similar models are restricted by the mean-field approximation. In the critical conditions near the phase transition, dissociation of hadrons and correlation of pre-hadron states can also contribute to the system thermodynamics. In [62], the two-particle correlation thermodynamics are described by a generalized Bethe–Uhlenbeck equation, which enables estimating the contributions from pre-hadron states to the system pressure near a phase transitions.

The structure of this review is as follows. In Section 2, the incorporation of the confinement properties into the chiral NJL model via the introduction of quark interaction with a background gauge field is described. The mass spectrum of the model and the structure of the QCD phase diagram corresponding to the Polyakov-loop extended NJL model are discussed. It is shown which interaction parameters can affect the phase diagram structure. In Section 3, the thermodynamic properties of nuclear matter described by this model are explored. Thermodynamic properties of quark matter are presented and a procedure for including meson correlations is proposed. In Section 4, we briefly consider the problems that were not covered in Section 2: inclusion of a minimal chemical potential into the model, a nonlocal PNJL model, and the effect of magnetic fields on the phase diagram structure.

2. Chiral models in QCD with confinement

2.1 Effective potential

The PNJL Lagrangian for scalar and pseudoscalar interactions with two quark flavors has the form [34, 35]

$$\mathcal{L}_{\mathrm{PNJL}} = \bar{q}(\mathrm{i}\gamma_\mu D^\mu - \hat{m}_0)q + G_\mathrm{s}\left[(\bar{q}q)^2 + (\bar{q}\,\mathrm{i}\gamma_5\tau q)^2\right] - \mathcal{U}(\Phi, \bar{\Phi}; T)\,. \quad (1)$$

This includes the four-quark interaction of quark fields q and $\bar{q}$, characteristic of the PNJL model with a coupling constant G_s, τ denotes the Pauli matrices in the flavor space, and $\hat{m}_0$ is the diagonal matrix of current quark masses. Coupling to the gauge field appears via the covariant derivative $D^\mu = \partial^\mu - \mathrm{i}A^\mu$ (A^μ is the gauge field) and the effective potential $\mathcal{U}(\Phi, \bar{\Phi}; T)$ depending on the complex field Φ of a Polyakov loop.

As is well known, QCD predicts a linearly increasing interaction between color objects at large distances. Therefore, it is possible to imagine that a quark and an antiquark created at some point x pass some distance before annihilating at some point x'. In this picture, the quark–antiquark trajectory is a loop, which is described in QCD by the Wilson

operator [63]

$$W(\bar{x}) = \mathrm{tr}\left[\mathcal{P}\left(\mathrm{i}g_\mathrm{s}\int_C A_\mu\,\mathrm{d}x_\mu\right)\right], \tag{2}$$

where A_μ is the total color vector potential of quarks and the vacuum, $\mathcal{P}$ is the ordering operator along the loop, g_s is the strong coupling constant, and the trace tr is taken over color indexes, because the quark–antiquark pair was created and annihilated in a colorless state. In this case, in the absence of dynamical quarks, the Wilson line is the order parameter determining the confinement.

For practical applications at finite temperatures and densities, confinement can be conveniently described by the Polyakov loop [63, 64]

$$l(\mathbf{x}) \equiv \mathrm{tr}\left[\mathcal{P}\exp\left(\mathrm{i}\int_0^\beta \mathrm{d}\tau\, A_4(\mathbf{x},\tau)\right)\right], \tag{3}$$

where $A_4 = \mathrm{i}A^0$ is the time component of the gauge field $(\mathbf{A}, A_4)$, which includes the constant g_s: $A^\mu(x) = g_\mathrm{s}A^\mu_a(\lambda_a/2)$, where A^μ_a is an SU(3) gauge filed and λ_a are the Gell-Mann matrices.

The Polyakov loop can be interpreted in analogy with the free energy $F_\mathrm{q}(\mathbf{x})$ [29, 35, 64] that has to be spent in order to add a heavy color source (a dynamical quark):

$$\langle l(\mathbf{x})\rangle = \exp\left(-\beta\Delta F_\mathrm{q}(\mathbf{x})\right).$$

If the system is closed, the amount of energy spent should be infinitely large; therefore, $\langle l(\mathbf{x})\rangle = 0$ corresponds to the confinement phase (Z_3-symmetric phase). If there is a color source in the system, the field Φ emerges that in the $\mathrm{SU_c}(3)$-gauge theory is introduced as the expectation value of the Polyakov line in a finite space volume [65]:

$$\Phi(\mathbf{x}) \equiv \langle\langle l(\mathbf{x})\rangle\rangle = \frac{1}{N_\mathrm{c}}\,\mathrm{tr}\,\langle\langle L(\mathbf{x})\rangle\rangle, \tag{4}$$

where $L(\mathbf{x})$ is the expression in brackets in the right-hand side of (2).

In the pure-gauge $\mathrm{SU}(N_\mathrm{c})$ theory, confinement is described by an effective potential that can be related to the Polyakov loop complex field [35, 64, 65]. The effective potential $U(\Phi,\bar{\Phi};T)$ for the PNJL model can be determined from the lattice QCD results obtained in the absence of dynamical quarks. The effective potential is subjected to two constraints: it must satisfy the Z_3-symmetry conditions and it must reproduce the results of gluodynamics in lattice QCD [66]. This gives a certain freedom in choosing the approximating function to describe the effective potential [34, 36, 38, 67].

• A polynomial from of the potential is most frequently used [34]:

$$\frac{\mathcal{U}_\mathrm{RTW05}(\Phi,\bar{\Phi};T)}{T^4} = -\frac{b_2(T)}{2}\,\bar{\Phi}\Phi - \frac{b_3}{6}(\Phi^3+\bar{\Phi}^3) + \frac{b_4}{4}(\bar{\Phi}\Phi)^2, \tag{5}$$

$$b_2(T) = a_0 + a_1\left(\frac{T_0}{T}\right) + a_2\left(\frac{T_0}{T}\right)^2 + a_3\left(\frac{T_0}{T}\right)^3. \tag{6}$$

• The highest-degree terms in (5) can be replaced by a logarithmic dependence [36, 67]:

$$\frac{\mathcal{U}_\mathrm{RTW06}(\Phi,\bar{\Phi};T)}{T^4} = -\frac{1}{2}\,a(T)\Phi\bar{\Phi} + b(T)\ln h(\Phi,\bar{\Phi}). \tag{7}$$

• Another approximating function was proposed in [38]:

$$\frac{\mathcal{U}_\mathrm{FU08}(\Phi,\bar{\Phi};T)}{bT} = -54\exp\left(-\frac{a}{T}\right)\Phi\bar{\Phi} + \ln h(\Phi,\bar{\Phi}). \tag{8}$$

• To study hadron matter in neutron stars, an explicit dependence of the effective potential on the chemical potential μ was introduced [68, 69]:

$$\frac{\mathcal{U}_\mathrm{DS09}(\Phi,\bar{\Phi};T)}{bT} = \left(a_0 + a_1\frac{\mu^4}{T^4} + a_2\frac{\mu^2}{T^2}\right)\Phi\bar{\Phi} + a_3\left(\frac{T_0}{T}\right)^4\ln h(\Phi,\bar{\Phi}). \tag{9}$$

In formulas (6)–(9),

$$h(\Phi,\bar{\Phi}) = 1 - 6\bar{\Phi}\Phi + 4(\bar{\Phi}^3+\Phi^3) - 3(\bar{\Phi}\Phi)^2,$$
$$a(T) = \tilde{a}_0 + \tilde{a}_1\left(\frac{T_0}{T}\right) + \tilde{a}_2\left(\frac{T_0}{T}\right)^2, \tag{10}$$
$$b(T) = \tilde{b}_3\left(\frac{T_0}{T}\right)^3,$$

and T_0, a_i, b_i, $\tilde{a}_i$, and $\tilde{b}_i$ are model parameters. The parameter T_0 depends on the number of flavors and the chemical potential, but $T_0 = 0.27$ in the pure-gauge sector [70].

To determine the model parameters and the effective potential, the following condition should be taken into account: $\Phi \to 1$ and $P/T^4 \to 1.75$ [the Stephan–Boltzmann (SB) limit for gluons] as $T \to \infty$. This immediately implies that $\tilde{a}_0 = 3.51$ for the logarithmic function in potential (7) and $a_0/2 + b_3/3 - b_4/4 = 1.75$ for polynomial function (5). By minimizing $\mathcal{U}(\Phi,\bar{\Phi},T)$ in Φ, taking into account that $\Phi = \bar{\Phi}$ at $\mu = 0$, and using the least-square method, the remaining coefficients in the effective potential can be found.

To approximate the potential, the lattice calculations data obtained in [66] and shown in Fig. 1 by the filled triangles are used. In 2009, the effective potential was calculated in [70] (the unfilled circles in Fig. 1). Calculating the parameters of the polynomial and logarithmic potentials that reproduce these data allows assessing how the parameterization of the effective potential affects the thermodynamics of hadrons. The obtained coefficients are listed in Table 1.

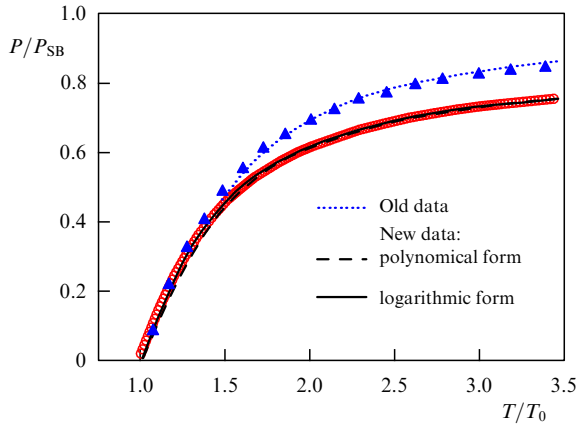

Figure 1. Normalized gluon pressure P/P_SB as a function of the normalized temperature. Old [66] and new [70] lattice data are respectively shown by filled triangles and circles. The dotted line shows a polynomial approximation of the old data. The solid and dashed line corresponds to the logarithmic and polynomial potential approximation.

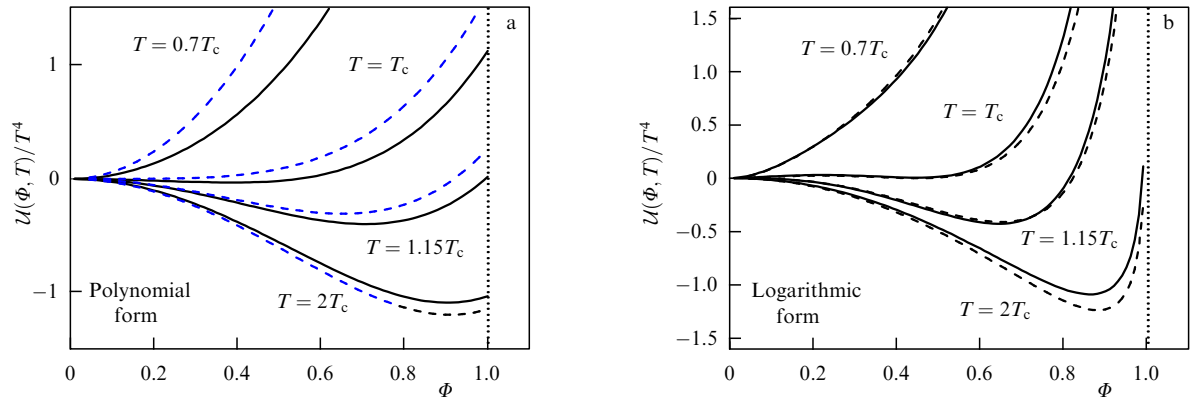

Figure 2. Effective potential $\mathcal{U}$ of the (a) polynomial and (b) logarithmic form as a function of Φ for different temperatures for old (dashed curves) and new (solid curves) parameters.

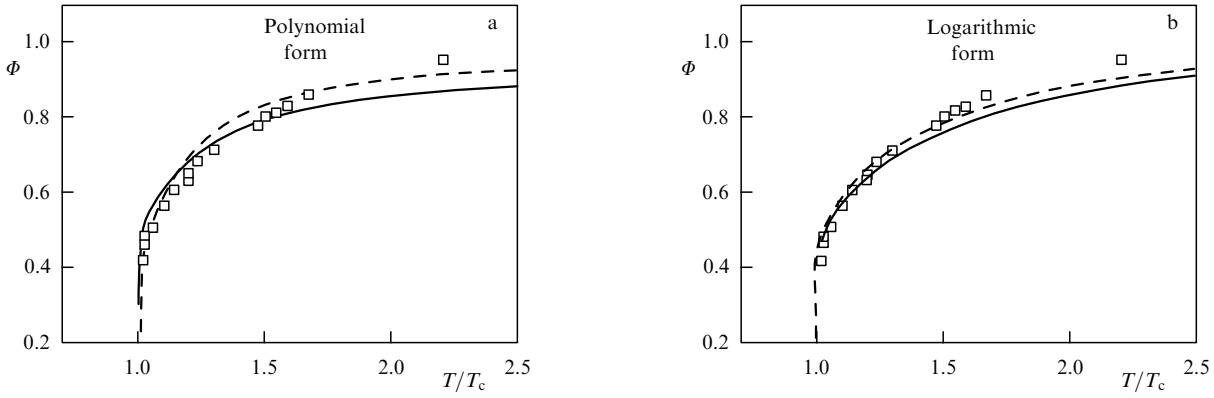

Figure 3. Polyakov loop field Φ for (a) polynomial (5) and (b) logarithmic (7) effective potentials. The solid (dashed) curve corresponds to the new (old) parameters. (Lattice data from [72].)

Table 1. Parameters of the effective potential $\mathcal{U}(\Phi, \bar{\Phi}; T)$ in polynomial and logarithmic approximations.

Data	Polynomial						Logarithmic			
	a_0	a_1	a_2	a_3	b_3	b_4	$\tilde{a}_0$	$\tilde{a}_1$	$\tilde{a}_2$	$\tilde{b}_3$
Old [66]	6.75	−1.95	2.625	−7.44	0.75	7.5	3.51	−2.47	15.2	−1.75
New [70]	6.47	−4.62	7.95	−9.09	1.03	7.32	3.51	−5.121	20.99	−2.09

The results of the approximation are also shown in Fig. 1. It is seen that the original lattice QCD data are quite different, by about 10% for $T/T_0 \sim 2$, while the logarithmic and polynomial approximations of the effective potential with fitted parameters are in very good agreement.

Figure 2 shows the effective potential $\mathcal{U}(\Phi, \bar{\Phi}; T)$ as a function of the field Φ for different temperatures. The figure implies that the way of describing the effective potential and its parameterization does not truly affect the general behavior of the potential. When the system is in the confinement state (the Z_3-symmetric phase), i.e., for temperatures below the critical 0.27 GeV value for gluons, the potential has a single minimum at $\Phi = 0$. As the temperature tends to the critical value, the effective potential flattens. At temperatures above the critical one, when the Z_3-symmetry is broken and deconfinement occurs in the system, the potential minimum occurs already at $\Phi \neq 0$. In the limit $T \to \infty$, the location of the minimum tends to 1. The applicability domain of the model with a Polyakov loop is restricted by the temperature $T \sim 2.5T_0$ [71].

A comparison of the Polyakov loop field with lattice QCD calculations is shown in Fig. 3. It is seen that irrespective of the potential approximation, the values of Φ obtained from the new data are somewhat smaller than those obtained from old data. This can be explained by noticing from Fig. 1 that the pressures obtained from the new and old data are significantly different. Although, strictly speaking, the Polyakov loop ceases to be an order parameter when a dynamical color charge (quark) appears in the vacuum, it remains a phase indicator for a large number of colors N_c (and even for $N_c = 2, 3$).

2.2 Constituent quarks and mesons

The Lagrangian of the PNJL model with a finite chemical potential has the form

$$\mathcal{L}_{\text{PNJL}} = \bar{q}(\mathrm{i}\gamma_\mu D^\mu - \hat{m}_0 + \gamma_0\mu)q + G_s\left[(\bar{q}q)^2 + (\bar{q}\,\mathrm{i}\gamma_5\tau q)^2\right] - \mathcal{U}(\Phi, \bar{\Phi}; T)\,, \tag{11}$$

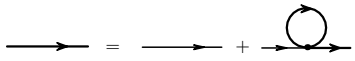

Figure 4. The Schwinger–Dyson equation in the Hartree approximation in diagram form. The thin solid line corresponds to the current quark propagator and the thick solid line shows the 'dressed' quark propagator. The loop describes the quark self-energy.

where G_s is the constant of the local scalar–pseudoscalar four-point interaction of the quark fields q and $\bar{q}$, τ is the Pauli matrices in the flavor space, and $\hat{m}_0$ is the diagonal matrix of the current quark masses $m_u^0 = m_d^0 = m_0$. Quarks are coupled to the gauge field by the covariant derivative $D^\mu = \partial^\mu - iA^\mu$ with $A^\mu(x) = g\mathcal{A}_a^\mu \lambda_a/2$, where $\mathcal{A}_a^\mu$ are fields in the pure-gauge SU(3) theory, λ_a are the Gell-Mann matrices, and $A^\mu = \delta_0^\mu A^0 = -i\delta_4^\mu A_4$ are gauge fields in the Polyakov gauge.

The quark self-energy caused by the interaction terms in the Lagrangian is calculated in the Hartree approximation. The corresponding Schwinger–Dyson equation in diagram form is presented in Fig. 4. This interaction leads to the appearance of a constant shift in the quark mass, and in the momentum representation, the equation takes the form

$$m = m_0 - 2iG_s \int \frac{d^4p}{(2\pi)^4} \operatorname{tr} S(p)\,, \tag{12}$$

where m_0 is the current quark mass,

$$iS(p) = i\,\frac{1}{\hat{p} + \gamma_0(-iA_4 + \mu) + m} \tag{13}$$

is the propagator of the 'dressed' quark (solid line), and the trace is taken over the color, flavor, and Dirac indices. In analogy with the BCS theory, Eqn (12) is frequently referred to as the gap equation, and the mass m is called the constituent quark mass. This equation is related to the quark condensate

$$\langle \bar{q}q \rangle = i \int \frac{d^4p}{(2\pi)^4} \operatorname{tr} S(p)\,, \tag{14}$$

with which Eqn (12) takes the form

$$m = m_0 + 2G_s\langle \bar{q}q \rangle\,,$$

whence the spontaneous chiral symmetry breaking mechanism is clearly seen: the quarks moving in a background gauge field acquire mass by adding the quark condensate. After taking the trace over Dirac and flavor indices and making the Matsubara replacement

$$\int \frac{dp_0}{2\pi} \int \frac{d^3p}{(2\pi)^3} \to iT \sum_{n=-\infty}^{+\infty} \int \frac{d^3p}{(2\pi)^3}\,, \tag{15}$$

we arrive at the equation

$$m = m_0 + 8N_f G_s m\, iT \sum_{n=-\infty}^{\infty} \int \frac{d^3p}{(2\pi)^3} \frac{1}{\left[\hat{p} + \gamma_0(-iA_4 + \mu)\right]^2 - m^2} \tag{16}$$

with a four-momentum $\hat{p} = \gamma_0 p_0 - \boldsymbol{\gamma}\mathbf{p}$, where $p_0 = i\omega_n - (iA_4 + \mu)$, $\omega_n = (2n+1)\pi T$ is the Matsubara frequency, and m is the quark mass. After the Matsubara summation, summation over the color indices is performed, which leads to the appearance of modified Fermi functions:

$$\begin{aligned}
&\operatorname{tr}_j\left\{f\left[E_p - (-iA_{4jj} + \mu)\right]\right\} \\
&= \sum_{j=1}^{N_c} \frac{1}{\exp\left[\beta(E_p - \mu)\right]\exp\left(i\beta A_{4jj}\right) + 1} \\
&= \Big[\left(\exp\left[\beta(E_p - \mu)\right]\exp\left(i\beta A_{422}\right) + 1\right) \\
&\times \left(\exp\left[\beta(E_p - \mu)\right]\exp\left(i\beta A_{433}\right) + 1\right) \\
&+ \left(\exp\left[\beta(E_p - \mu)\right]\exp\left(i\beta A_{411}\right) + 1\right) \\
&\times \left(\exp\left[\beta(E_p - \mu)\right]\exp\left(i\beta A_{433}\right) + 1\right) \\
&+ \left(\exp\left[\beta(E_p - \mu)\right]\exp\left(i\beta A_{411}\right) + 1\right) \\
&\times \left(\exp\left[\beta(E_p - \mu)\right]\exp\left(i\beta A_{422}\right) + 1\right)\Big] \\
&\times \Big[\left(\exp\left[\beta(E_p - \mu)\right]\exp\left(i\beta A_{411}\right) + 1\right) \\
&\times \left(\exp\left[\beta(E_p - \mu)\right]\exp\left(i\beta A_{422}\right) + 1\right) \\
&\times \left(\exp\left[\beta(E_p - \mu)\right]\exp\left(i\beta A_{433}\right) + 1\right)\Big]^{-1} \\
&= N_c\Big\{\bar{\Phi}\exp\left[-\beta(E_p - \mu)\right] + 2\Phi\exp\left[-2\beta(E_p - \mu)\right] \\
&+ \exp\left[-3\beta(E_p - \mu)\right]\Big\} \\
&\times \Big\{1 + 3\left(\bar{\Phi} + \Phi\exp\left[-\beta(E_p - \mu)\right]\right)\exp\left[-\beta(E_p - \mu)\right] \\
&+ \exp\left[-3\beta(E_p - \mu)\right]\Big\}^{-1} = N_c f_\Phi^+(E_p - \mu)\,.
\end{aligned} \tag{17}$$

Similarly,

$$\begin{aligned}
&\operatorname{tr}_j\left\{f\left[E_p + (-iA_{4jj} + \mu)\right]\right\} \\
&= N_c\Big\{\Phi\exp\left[-\beta(E_p + \mu)\right] + 2\bar{\Phi}\exp\left[-2\beta(E_p + \mu)\right] \\
&+ \exp\left[-3\beta(E_p + \mu)\right]\Big\} \\
&\times \Big\{1 + 3\left(\Phi + \bar{\Phi}\exp\left[-\beta(E_p + \mu)\right]\right)\exp\left[-\beta(E_p + \mu)\right] \\
&+ \exp\left[-3\beta(E_p + \mu)\right]\Big\}^{-1} = N_c f_\Phi^-(E_p + \mu)\,.
\end{aligned} \tag{18}$$

In expressions (17) and (18), $N_c = 3$ and $f_\Phi^\pm$ are the modified Fermi functions.

As a result, we obtain the equation

$$m = m_0 + 8G_s N_f N_c\, im \int \frac{d^3p}{(2\pi)^3} \frac{1}{E_p}\left(1 - f_\Phi^+(E_p) - f_\Phi^-(E_p)\right), \tag{19}$$

where N_f is the number of flavors. The NJL model can be considered the limit case of the PNJL model as $\Phi = \bar{\Phi} \to 1$.

Mesons in the PNLJ model are introduced as collective modes (quark–antiquark bound states). The meson propagator in the random phase approximation (Fig. 5) is defined in terms of the T-matrix as

$$T_M(k^2) = \frac{2iG_s}{1 - 2G_s\Pi_M(k^2)}\,. \tag{20}$$

Figure 5. Effective interaction in the random phase approximation. On the left-hand side, the double-dashed line denotes the meson propagator. The solid lines stand for quark lines; circles denote the quark–meson coupling constant.

All information on the meson properties is contained in the function Π_M called the polarization operator of mesons

$$\Pi_M(k^2) = \mathrm{i}\int \frac{\mathrm{d}^4 p}{(2\pi)^4}\ \mathrm{tr}\left[\Gamma_M S(p+k)\Gamma_M S(p)\right], \tag{21}$$

where $S(p)$ is quark propagator (13) and Γ_M corresponds to the vertex function of a given meson: $\Gamma_\pi = \mathrm{i}\gamma_5\tau^a$ for a π-meson and $\Gamma_\sigma = \mathbf{1}$ for a σ-meson.

In the pole approximation, the matrix T_M can be represented in the form

$$T_M = \frac{g_{Mqq}^2}{k^2 - m_M^2}\,. \tag{22}$$

By comparing (22) with (20), we see that to find the mass of a meson m_M, we must solve the equation

$$1 - 2G_\mathrm{s}\Pi_M(k^2)\big|_{k^2=m_M^2} = 0\,, \tag{23}$$

and the meson–quark coupling constant is calculated as

$$g_{Mqq}^{-2} = \left.\frac{\partial\Pi_M(k^2)}{\partial k^2}\right|_{k^2=m_M^2}. \tag{24}$$

For mesons in the rest frame ($k = 0$), equations for their mass have the form

$$1 - 8N_\mathrm{c}N_\mathrm{f}G_\mathrm{s}I_1 + 2N_\mathrm{c}N_\mathrm{f}G_\mathrm{s}k^2 I_2(k^2)\big|_{k^2=m_\pi^2} = 0\,, \tag{25}$$

$$1 - 8N_\mathrm{c}N_\mathrm{f}G_\mathrm{s}I_1 + 2N_\mathrm{c}N_\mathrm{f}G_\mathrm{s}(k^2 - 4m^2)I_2(k^2)\big|_{k^2=m_\sigma^2} = 0\,, \tag{26}$$

where

$$I_1 = \int \frac{p^2\,\mathrm{d}p}{4\pi^2}\,\frac{1}{E_p}\left(1 - f_\Phi^+(E_p) - f_\Phi^-(E_p)\right), \tag{27}$$

$$I_2(k^2) = \int \frac{p^2\,\mathrm{d}p}{2\pi^2}\,\frac{1}{E(k^2 - 4E_p^2)}\left(1 - f_\Phi^+(E_p) - f_\Phi^-(E_p)\right). \tag{28}$$

The dependence of the meson masses and double quark mass on temperature is shown in Fig. 6 for two approximations of the effective potential and two parameter sets from Table 1. Clearly, for the polynomial effective potential, the results for the old and new parameters differ more than for the logarithmic approximation.

2.3 Grand thermodynamic potential. Mean-field approximation

To describe thermodynamic properties of a system with a variable number of particles, the definition of a canonical ensemble is required. Here, the partition function is defined as a sum over all eigenenergies of the QCD Hamiltonian and can be expressed via the generating functional

$$\mathcal{Z} = \sum_\alpha \exp\left[-\beta(E_\alpha - \mu_\mathrm{b}B_\alpha)\right], \tag{29}$$

where β is the inverse temperature, α is a state with the baryon number B_α and energy E_α, and μ_b is the baryon chemical potential. On the other hand, in the imaginary time formalism with $\tau = \mathrm{i}t$, the generating functional has the form

$$\mathcal{Z}[T, V, \mu] = \int \mathcal{D}\bar{q}\mathcal{D}q \exp\left(\int_0^\beta \mathrm{d}\tau \int_v \mathrm{d}^3x\,\mathcal{L}_\mathrm{PNJL}\right). \tag{30}$$

After applying the Hubbard–Stratonovich transformation, auxiliary meson fields are introduced, and the functional takes the form

$$\mathcal{Z}[T, V, \mu] = \int \mathcal{D}\sigma'\mathcal{D}\pi'\mathcal{D}\bar{q}\mathcal{D}q \exp\left[\int \mathrm{d}^4x\left(\mathcal{L}'_\mathrm{PNJL} - \frac{\sigma'^2 + \pi'^2}{4G_\mathrm{s}}\right)\right] \times \exp\left(-\int \mathrm{d}^4x\,\mathcal{U}(\Phi, \bar{\Phi}; T)\right). \tag{31}$$

For the simplest estimate, the mean field (MF) approximation is used, in which the meson fields are described as fluctuations about the mean value $\sigma' = \sigma + \sigma_\mathrm{MF}$ and $\pi' = \pi + \pi_\mathrm{MF}$. Retaining only terms relating to the mean field, we obtain the functional

$$\mathcal{Z}_\mathrm{MF} = \exp\left[\int \mathrm{d}^4x\left(-\frac{\sigma'^2_\mathrm{MF}}{4G_\mathrm{s}}\right) + \mathrm{tr}\ln S_\mathrm{MF}^{-1}(m) - \frac{V}{T}\,\mathcal{U}(\Phi, \bar{\Phi}; T)\right]. \tag{32}$$

Then the grand thermodynamic potential for the PNJL model in the MF approximation has the form

$$\Omega_\mathrm{PNJL}(T, \mu) = -\frac{T}{V}\ln\mathcal{Z}_\mathrm{MF}[T, V, \mu]\,, \tag{33}$$

$$\Omega_\mathrm{PNJL} = \mathcal{U}(\Phi, \bar{\Phi}; T) + G_\mathrm{s}\langle\bar{q}q\rangle^2 + \Omega_\mathrm{q} \tag{34}$$

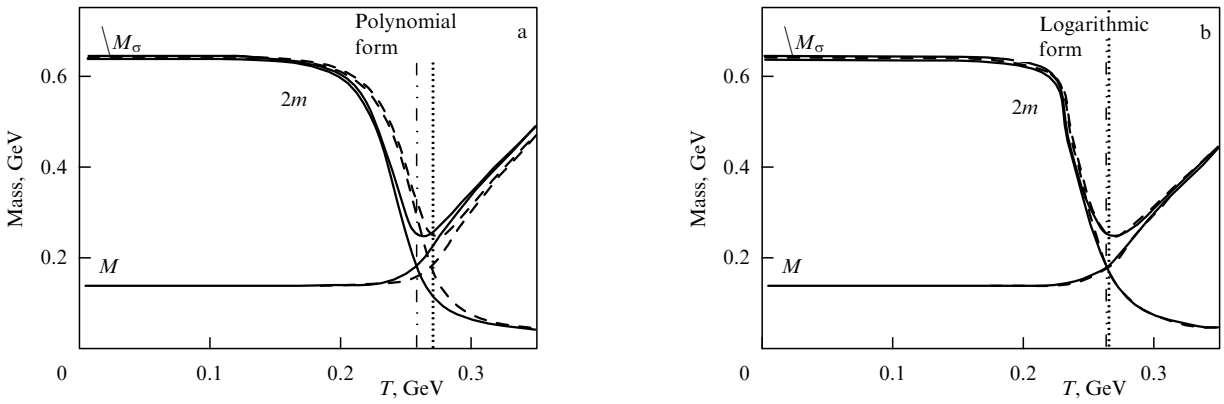

Figure 6. Temperature dependence of the double quark masses and meson masses for the (a) polynomial and (b) logarithmic parameterization of the old and new effective potential (respectively shown by the solid and dashed lines). The vertical lines show the Mott temperature T_Mott.

with the quark part

$$\Omega_{\rm q} = -2N_{\rm c}N_{\rm f}\int\frac{{\rm d}^3p}{(2\pi)^3}E_p - 2N_{\rm f}T\int\frac{{\rm d}^3p}{(2\pi)^3}\,{\rm tr}_{\rm c}\left[\ln\left(1+L^{\dagger}\exp\left[-\beta(E_p-\mu)\right]\right) + \ln\left(1+L\exp\left[-\beta(E_p+\mu)\right]\right)\right]. \quad (35)$$

The integrand in (35) contains the sum of the functions

$$N_{\Phi}^{+}(E_p) = {\rm tr}_{\rm c}\left[\ln\left(1+L^{\dagger}\exp\left[-\beta(E_p-\mu)\right]\right)\right] = 1+3\left(\Phi+\bar{\Phi}\exp\left(-\beta E_p^{+}\right)\right)\exp\left(-\beta E_p^{+}\right)+\exp\left(-3\beta E_p^{+}\right), \quad (36)$$

$$N_{\Phi}^{-}(E_p) = {\rm tr}_{\rm c}\left[\ln\left(1+L\exp\left[-\beta(E_p+\mu)\right]\right)\right] = 1+3\left(\bar{\Phi}+\Phi\exp\left(-\beta E_p^{-}\right)\right)\exp\left(-\beta E_p^{-}\right)+\exp\left(-3\beta E_p^{-}\right), \quad (37)$$

where $E_p^{\pm} = E_p \mp \mu$, $\beta = 1/T$, and the quark energy is defined as $E_p = (\mathbf{p}^2+m^2)^{1/2}$.

Because spontaneous chiral symmetry breaking is accompanied by the appearance of massive quarks in the system, the quark mass (or the quark condensate) is an order parameter of the chiral phase transition. At the same time, the Polyakov loop field $\Phi\,(\bar{\Phi}\,)$ is an order parameter of the confinement–deconfinement phase transition. Correspondingly, the system thermal equilibrium condition is given by

$$\frac{\partial\Omega_{\rm PNJL}}{\partial\langle\bar{q}q\rangle}=0\,,\qquad \frac{\partial\Omega_{\rm PNJL}}{\partial\Phi}=0\,,\qquad \frac{\partial\Omega_{\rm PNJL}}{\partial\bar{\Phi}}=0\,, \quad (38)$$

and the first condition again leads to the gap equation $m = m_0 + 2G_{\rm s}\langle\bar{q}q\rangle$.

To illustrate processes of symmetry restoration and breaking, Fig. 7 shows the behavior of the Polyakov loop field Φ and the quark condensate normalized to the zero-temperature value, $\langle\bar{q}q\rangle/\langle\bar{q}q\rangle_0$, as a function of temperature for the PNJL model at $G_{\rm v}=0$. The appearance of a dynamic quark decreases the slope of Φ in the transition region, compared to its slope in the gulodynamic case (see Fig. 3). Figure 7 shows that at low temperatures, when $\Phi\sim 0$, confinement is observed in the system, and the Z_3-symmetry is apparently restored. But, at the same time, the chiral symmetry is spontaneously broken, which is due to the quarks having nonzero constituent mass in hadrons. After the transition region, the quark mass becomes a current one, which leads to partial chiral symmetry restoration (the chiral symmetry restoration cannot be complete because the current quark masses are nonzero). Meanwhile, the field Φ becomes nonzero, which leads to Z_3-symmetry violation and, as a consequence, to deconfinement. Lattice QCD studies showed that these transitions should occur at one temperature [72, 73].

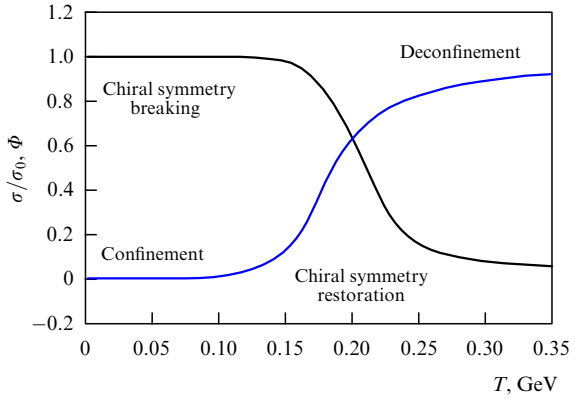

Figure 7. (Color online.) Temperature dependence of the normalized quark condensation σ/σ_0 (black curve) and the Polyakov loop field Φ (blue curve).

2.4 Phase diagram of hadron matter in the PNJL model

We can now discuss the structure of the QCD phase diagram of hadron matter in NJL-type models with the Polyakov loop. Thermodynamic equilibrium conditions are given by Eqns (38). Traditionally, in the NJL and PNJL models, the line of the phase transition from the spontaneously broken chiral state to the restored chiral symmetry state (the chiral phase transition) at low temperatures is determined as the maximum of the derivative $\partial\langle\bar{q}q\rangle/\partial T|_{\mu={\rm const}}$. The phase transition point from confinement to deconfinement is determined as $\max\left(\partial\Phi/\partial T\right)$ at $\mu={\rm const}$ [34, 36]. At low temperatures, the PNJL model, as well as the NJL model, demonstrates a crossover — a soft phase transition characterized by a considerable increase in the order parameter. As the chemical potential increases, three roots appear in the gap equation solution, and finding the phase transition line by the above means becomes impossible. The appearance of three roots suggests a first-order phase transition in the system. In this case, the first-order phase transition is defined in terms of the quark susceptibility [74] introduced as

$$\frac{\chi_{\rm q}(T,\mu)}{T^2}=\frac{\partial^2(p/T^4)}{\partial(\mu/T)^2}=\frac{\partial}{\partial(\mu/T)}\left(\frac{\rho}{T^3}\right). \quad (39)$$

The first-order phase transition region ends at a temperature at which $\chi_{\rm q}$ as a function of the chemical potential demonstrates a sharp maximum; this is the critical end point (CEP). At temperatures below $T_{\rm CEP}$, $\chi_{\rm q}$ has a discontinuity as a function of the chemical potential. At temperatures above $T_{\rm CEP}$, the discontinuity disappears, and $\chi_{\rm q}$ has a weak maximum. The behavior of the order parameters is shown in Fig. 8.

Figure 9 shows the phase diagrams of the PNJL model with effective potentials (5) and (7) with the old and new parameters from Table 1 and the free parameters $\Lambda = 0.639$ GeV, $m_0 = 5.5$ MeV, and $G_{\rm s} = 5.227$ GeV^{-2} at $T_0 = 0.27$ GeV. The figure shows that the critical temperature of the chiral phase transition at zero chemical potential is greatly overestimated in all cases: at zero chemical potential, the transition occurs at the temperatures $T_{\rm c} = 0.2395$, 0.253 GeV for the polynomial effective potential and at $T_{\rm c} = 0.23$, 0.234 GeV for the logarithmic potential with the new and old parameters, respectively. Clearly, the choice of parameters affects the model with the polynomial effective potential more strongly, but nevertheless the parameterization of the effective potential is less significant than the effective potential form for the phase diagram. The critical point location $(T_{\rm CEP}, \mu_{\rm CEP})$ is determined as (0.118, 0.3166) and (0.11, 03192) for the logarithmic, and (0.10, 0.3175) and (0.09, 0.322) for the polynomial approximations of the potential for the new and old parameters, respectively. It is seen that new parameters affect the critical point shift along

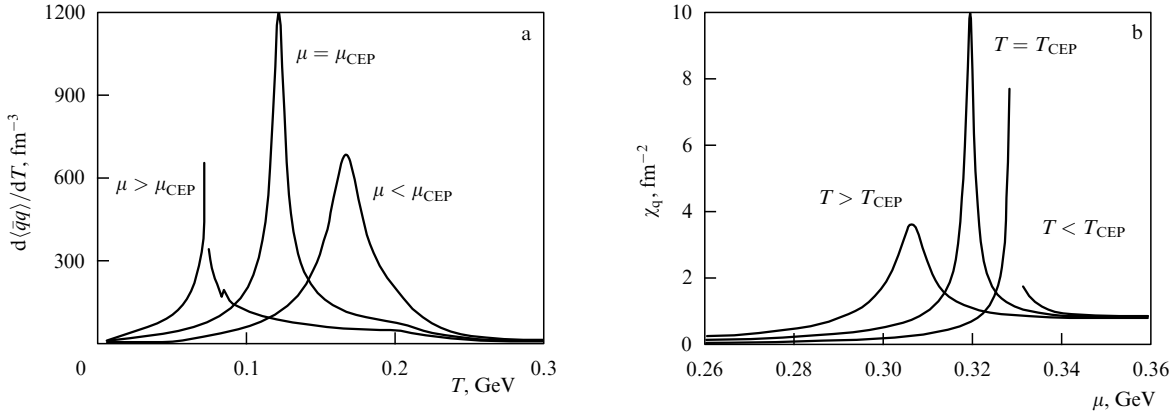

Figure 8. Behavior of the order parameters: (a) quark condensate and (b) quark susceptibility before, near, and beyond the CEP.

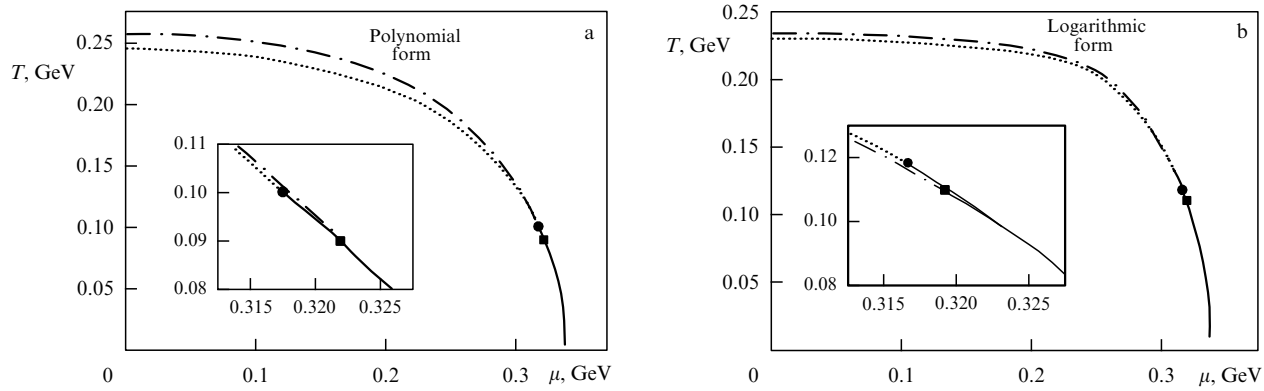

Figure 9. Phase diagram of the PNJL model with (a) polynomial and (b) logarithmic approximations of the effective potential. The solid curves show a first-order phase transition; the dashed and dashed-dotted lines indicate a crossover-like chiral phase transition. The filled circles mark the CEPs. The zoomed CEP region is shown in the insets.

the chemical potential more strongly than along the temperature shift.

The problem of the increased critical temperature at zero chemical potential in the PNJL model (0.23–0.253 GeV against 0.19 GeV in NJL and 0.17 GeV in the lattice calculations) was discussed in earlier papers devoted to the PNJL model [34, 36], where it was proposed to renormalize the parameter corresponding to the deconfinement temperature in the gluon sector from $T_0 = 0.270$ GeV to 0.19 GeV. This decreased the chiral phase transition temperature to 0.18–0.19 GeV, but then it ceases to coincide with the deconfinement temperature. To avoid that inconsistency, the phase transition temperature was taken to be the pseudocritical transition temperature at zero chemical potential, equal to the mean value of the chiral transition temperature and the deconfinement transition temperature. Nevertheless, this approach does not resolve the inconsistency between the two phase transition temperatures.

The search for the CEP is of great interest, but no consistency has been achieved here yet. For example, if a vector interaction is added to the model, it is possible to find parameters such that the first-order phase transition and the CEP disappear.

2.5 Vector interaction in the PNJL model

The inclusion of vector interaction in the NJL model was considered in [53, 54] and in the PNJL model, in [38, 55–60]. Vector interaction is introduced into the PNJL model by adding the term $G_v(\bar{q}\gamma_\nu q)^2$:

$$\mathcal{L}_{PNJL} = \bar{q}(i\gamma_\mu D^\mu - \hat{m}_0 - \gamma_0\mu)q + G_s\left[(\bar{q}q)^2 + (\bar{q}i\gamma_5\tau q)^2\right] - G_v(\bar{q}\gamma_\nu q)^2 - \mathcal{U}(\Phi, \bar{\Phi}; T)\,. \quad (40)$$

Here, G_v is the vector coupling constant and the other notation is the same as in (1).

The grand thermodynamic potential in the MF approximation with vector interaction is given by [34, 35]

$$\Omega(\Phi, \bar{\Phi}, m, T, \mu) = \mathcal{U}(\Phi, \bar{\Phi}; T) + G_s\langle\bar{q}q\rangle^2 + G_v\rho^2 + \Omega_q\,, \quad (41)$$

where $\langle\bar{q}q\rangle$ is the quark condensate, $\rho = \langle\bar{q}\gamma_0 q\rangle$ is the density of quarks, and the quark part is

$$\Omega_q = -2N_c N_f \int \frac{d^3p}{(2\pi)^3}\, E_p - 2N_f T \int \frac{d^3p}{(2\pi)^3}\left(\ln\tilde{N}^+_\Phi(E_p) + \ln\tilde{N}^-_\Phi(E_p)\right). \quad (42)$$

Here, the functions $\tilde{N}^\pm_\Phi$ differ from (36) and (37) by the appearance of a normalized chemical potential $\tilde{\mu}$:

$$\tilde{N}^+_\Phi = 1 + 3\left[\Phi + \bar{\Phi}\exp(-\beta E^+_p)\right]\exp(-\beta E^+_p) + \exp(-3\beta E^+_p)\,, \quad (43)$$

$$\tilde{N}^-_\Phi = 1 + 3\left[\bar{\Phi} + \Phi\exp(-\beta E^-_p)\right]\exp(-\beta E^-_p) + \exp(-3\beta E^-_p)\,, \quad (44)$$

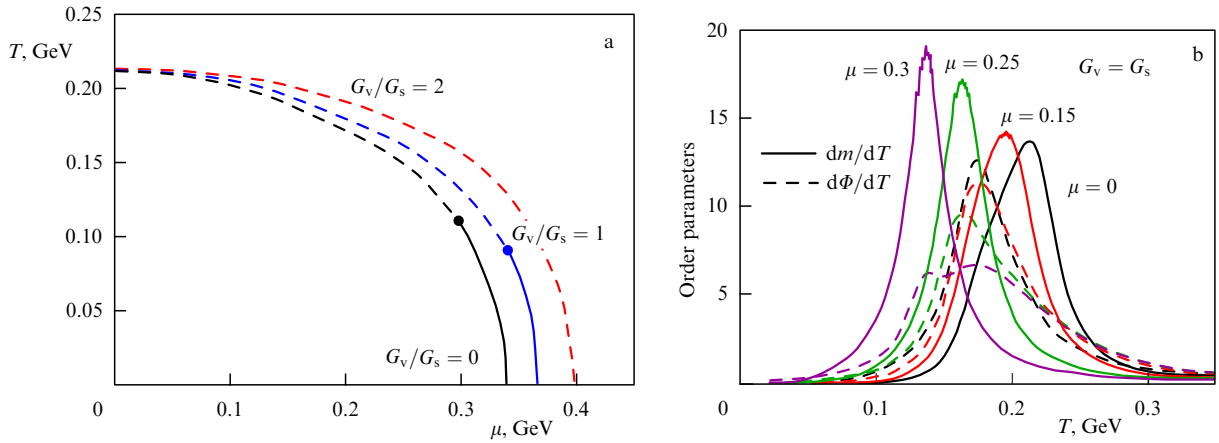

Figure 10. (a) The phase diagram of the PNJL model and vector interaction. (b) Order parameters of the NJL models with the Polyakov loop and vector interaction for $G_v = G_s$. The solid curves represent the order parameter of the chiral phase transition; the dashed lines show the order parameter of the confinement–deconfinement phase transition

where $E_p^{\pm} = E_p \mp \tilde{\mu}$, $E_p = \sqrt{\mathbf{p}^2 + m^2}$, and $\tilde{\mu}$ is expressed in terms of the quark chemical potential μ and the quark density as $\tilde{\mu} = \mu - 2G_v\rho$.

The thermodynamic equilibrium state of the system is now determined by four equations

$$\frac{\partial\Omega}{\partial\langle\bar{q}q\rangle} = 0\,, \quad \frac{\partial\Omega}{\partial\Phi} = 0\,, \quad \frac{\partial\Omega}{\partial\bar{\Phi}} = 0\,, \quad \frac{\partial\Omega}{\partial\tilde{\mu}} = 0\,.$$

As before, the first of these leads to the gap equation

$$m = m_0 + 4G_sN_cN_f\int_\Lambda \frac{d^3p}{(2\pi)^3}\frac{m}{E_p}\left(1 - \tilde{f}_\Phi^+(E_p) - \tilde{f}_\Phi^-(E_p)\right) \quad (45)$$

with the normalized chemical potential

$$\tilde{\mu} = \mu - 4G_vN_cN_f\int_\Lambda \frac{d^3p}{(2\pi)^3}\frac{m}{E_p}\left(\tilde{f}_\Phi^+(E_p) - \tilde{f}_\Phi^-(E_p)\right), \quad (46)$$

and the modified Fermi functions that also incorporate the normalized chemical potential

$$\tilde{f}_\Phi^+(E_p) = \frac{\left[\Phi + 2\bar{\Phi}\exp\left(-\beta E_p^+\right)\right]\exp\left(-\beta E_p^+\right) + \exp\left(-3\beta E_p^+\right)}{\tilde{N}_\Phi^+}\,, \quad (47)$$

$$\tilde{f}_\Phi^-(E_p) = \frac{\left[\bar{\Phi} + 2\Phi\exp\left(-\beta E_p^-\right)\right]\exp\left(-\beta E_p^-\right) + \exp\left(-3\beta E_p^-\right)}{\tilde{N}_\Phi^-}\,, \quad (48)$$

where $E_p^{\pm} = E_p \mp \tilde{\mu}$

Figure 10a shows the phase diagram of the PNJL model with vector interaction. The effective potential is chosen in the polynomial form with parameters from Table 1 and with $T_0 = 0.19$ GeV. As mentioned in Section 2.4, this normalization of the parameter decreases the critical temperature of the phase transition at zero chemical potential but causes the chiral phase transition and deconfinement to occur at different temperatures. This is seen from Fig. 10b, in which the model order parameters are also shown. Figure 10 also confirms that as the vector coupling constant increases, the first-order phase transition disappears.

The four-quark interaction G_s, which is present in the NJL and PNJL model Lagrangians, can be regarded as a diagram of gluon exchange between two quarks. The gluon field A_v and its time component A_0 are coupled to the Polyakov loop field [75], and G_s can be substituted by an effective vertex depending on Φ. Because the PNJL model respects an extended Z_3-symmetry,[1] it is possible to introduce a phenomenological dependence of $G_s(\Phi)$ [48]:

$$\tilde{G}_s(\Phi) = G_s\left[1 - \alpha_1\Phi\bar{\Phi} - \alpha_2(\Phi^3 + \bar{\Phi}^3)\right], \quad (49)$$

where parameters $\alpha_1 = \alpha_2 = 0.2$ are chosen such that the model reproduces the lattice QCD data at $\mu = 0$. This idea was later used in many papers [49, 50, 77] to explore the structure of the phase diagram without vector interaction. In [52, 78], it was first proposed that the dependence of the vector coupling constant on the Polyakov loop be included:

$$\tilde{G}_v(\Phi) = G_v\left[1 - \alpha_1\Phi\bar{\Phi} - \alpha_2(\Phi^3 + \bar{\Phi}^3)\right]. \quad (50)$$

The normalization of the vector coupling constant is chosen such that the constant ratio $\tilde{G}_v/\tilde{G}_s$ remains independent of Φ, and the same parameters α_1 and α_2 are used for $\tilde{G}_v$ and $\tilde{G}_s$.

Due to such an increase in the quark–gluon coupling, the renormalization of the parameter T_0 makes the phase transitions occur at the same temperature, and the phase transition temperature at zero chemical potential significantly decreases. This is seen from Fig. 11, in which the phase diagram and the order parameter are plotted. Figure 11 also implies that the vector coupling constant at which the first-order phase transition disappears is significantly larger in the model with a Φ-dependent vector coupling constant.

Lattice QCD calculations meet some difficulty at a finite chemical potential. This is related to the so-called sign problem [79], where the determinant of the mass operator becomes imaginary, which prevents Monte Carlo methods from being used. To extrapolate the results obtained at zero chemical potential to finite chemical potentials and to determine the CEP, the so-called 'crossover curvature' has been introduced. It is derived from the observation that critical curves for all physical quantities (chiral condensate, quark susceptibility, strange quark susceptibility, Polyakov

[1] As shown in [76], besides the Z_3-symmetry, QCD also incorporates a periodicity in the parameter Θ_q: $\Omega_{QCD}(\Theta_q) = \Omega_{QCD}(\Theta_q + 2\pi k/3)$, where k is an integer and $\mu_q = i\Theta_q T$. This combination was called the extended Z_3-symmetry. A series of papers on the PNJL model with imaginary chemical potentials proved that this model also respects the Z_3-symmetry.

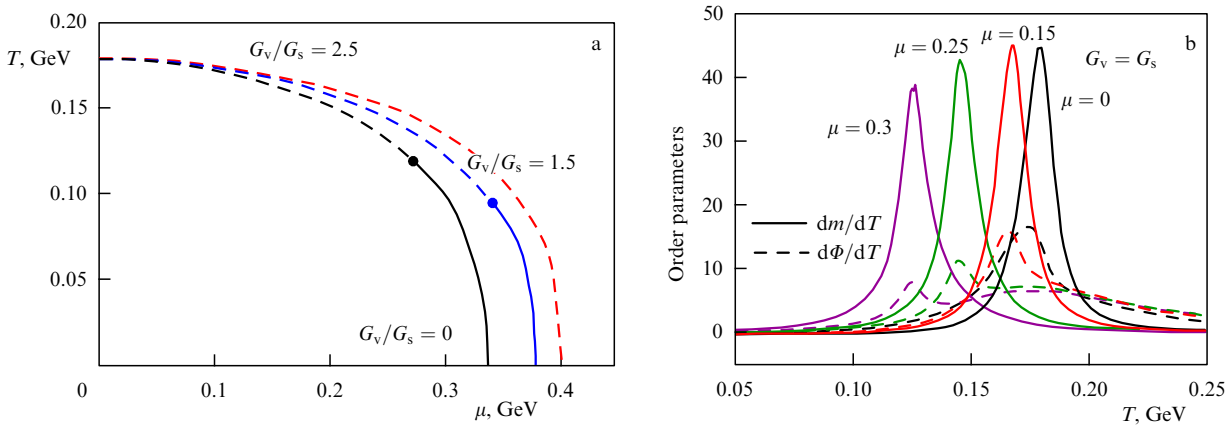

Figure 11. (a) Phase diagram of the PNJL model with vector interaction with the coupling constant depending on Φ. (b) Order parameters of the PNJL models with vector interaction for $G_v = G_s$ and the coupling constant depending on Φ. The solid curves represent the order parameter of the chiral phase transition; the dashed lines show the order parameter of the confinement–deconfinement phase transition.

loop) must converge at one point, which is the CEP:

$$\frac{T_c(\mu)}{T_c(0)} = 1 - k\left(\frac{\mu}{T_c(\mu)}\right)^2 . \tag{51}$$

In lattice QCD, this value is defined differently. For example, for $2+1$-flavor quarks, a Taylor series expansion in [80] yields $k = 0.059 \pm 0.020$; scaling the properties of the chiral condensate and chiral susceptibility respectively yields $k = 0.0089 \pm 0.0014$ and 0.0066 ± 0.002 [70], and calculations for the imaginary chemical potential yield $k = 0.0132 \pm 0.0018(0.003)$ [81]. Unfortunately, data for two flavors are almost absent. This can be explained by the fact that, as stated in some papers (e.g., [82]), the sign problem arises only in SU(3) models. The most precise is apparently the result for two degenerate fermions obtained in [43]: $k = 0.00563 \pm 0.00038$. But because the s-quark does not affect the system thermodynamics and only chemical potentials of light quarks are taken into account in calculations in the $2+1$-flavor case, the correspondence between the results obtained in the SU(2) PNJL model and in lattice QCD seems to be quite reasonable.

The calculations of the crossover for the PNJL model and the PNJL model with the coupling constant depending on the Polyakov loop are presented in Fig. 12 as a function of G_v/G_s. It is seen that, without vector interaction, the model results significantly exceed those of lattice QCD. With increasing the vector coupling constant, the crossover curvature becomes comparable with these results. This is seen especially well for the model with the vector coupling constant depending on Φ.

To summarize, in heavy-ion collisions, the hot nuclear matter can reach conditions when the quarks confined in hadrons become free: deconfinement occurs, which is accompanied by partial restoration of chiral symmetry, i.e., restoration of quark masses to their current values, much smaller than the quark masses in hadrons. Predictions of models with physical (i.e., nonzero) current quark masses suggest two possible scenarios of the transition from hadron matter to the quark–gluon plasma. At high temperatures and low matter densities, a soft phase transition (crossover) is assumed. At low temperatures and high chemical potentials (matter densities), a first-order phase transition is assumed. The point at which one phase transition is transformed into another is called the CEP. Present and future experiments are raising interest in the search for the CEP location on the

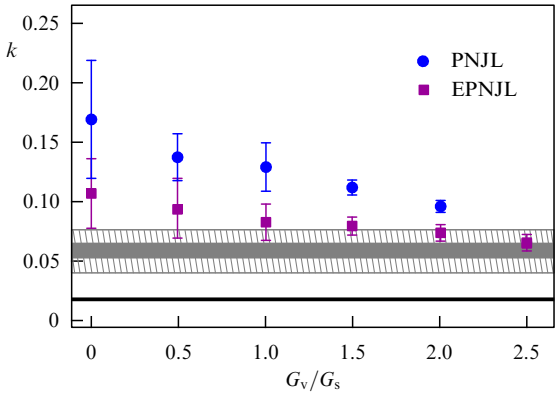

Figure 12. The crossover curvature k for the PJNL model and the PJNL model with Φ-dependent coupling constants (EPJNL) as a function of G_v/G_s. The gray and black stripes respectively show the $2+1$ quark flavor lattice QCD calculations obtained in [79, 83]. The broad hatched band corresponds to lattice QCD with an imaginary potential [80].

temperature–chemical-potential (quark or baryon) plane. Here, no consistency has been achieved yet. As an example, results of some theoretical models, including those discussed in this paper, and of lattice QCD calculations are presented in Fig. 13.

3. Equation of state of excited nuclear matter

3.1 Equation of state of quark matter

All other thermodynamic quantities can be derived from the grand thermodynamic potential Ω in (34): the pressure P, the energy density ε, the entropy density s, and the particle number density ρ:

$$P = -\frac{\Omega}{V} , \tag{52}$$

$$s = -\left(\frac{\partial\Omega}{\partial T}\right)_\mu , \tag{53}$$

$$\varepsilon = -P + Ts + \mu\rho , \tag{54}$$

$$\rho = -\left(\frac{\partial\Omega}{\partial\mu}\right)_T . \tag{55}$$

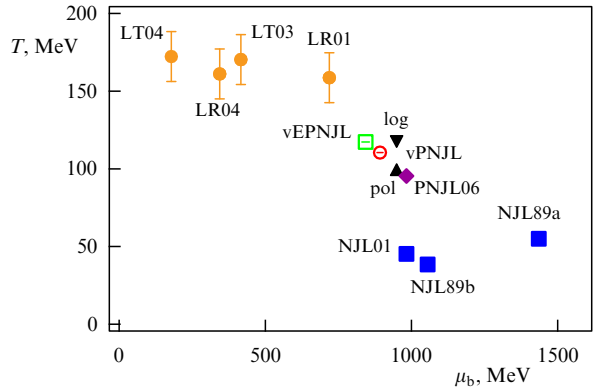

Figure 13. Comparison of the predicted location of the CEP on the phase diagram. Model predictions: NJL89a, NJL89b [84], NJL01 [85], PNJL [86]; log and pol mark the results obtained for the logarithmic and polynomial approximation of the effective potential; vPNJL and vEPNJL are the results in this section. The lattice QCD predictions: LT03 [86], LT04 [87], LR01 [88], LR04 [89].

The thermodynamic potential in the MF approximation has form (34) for the PNJL model and (41) for the PNJL model with vector interaction. In each case, the vacuum part can be separated:

$$\Omega_{\rm vac} = \frac{(m-m_0)^2}{4G} - 2N_{\rm c}N_{\rm f}\int\frac{{\rm d}^3p}{(2\pi)^3}\,E_p\,. \tag{56}$$

This quantity does not vanish as $T\to 0$ and $\mu\to 0$. Therefore, to obtain the physical value of the thermodynamic potential that would correspond to the pressure vanishing at zero temperature and density, $(T,\mu)=(0,0)$, it is necessary to renormalize the potential by extracting vacuum part (56). This leads to the following physical definition of pressure:

$$\frac{P}{T^4} = \frac{P(T,\mu,m)-P(0,0,m)}{T^4}\,. \tag{57}$$

Figure 14a shows the pressure obtained in the PNJL model with vector interaction and polynomial effective potential (5) with parameters from Table 1 at $T_0 = 0.19$ GeV, $\mu=0$, and $G_{\rm v}=0$. Figure 14b shows the pressure calculated in the PNJL model with vector interaction where the coupling constants depend solely on Φ.

As the temperature increases, the pressure should reach the Stephan–Boltzmann limit [91]

$$\frac{P_{\rm SB}}{T^4} = (N_{\rm c}^2-1)\,\frac{\pi^2}{45} + N_{\rm c}N_{\rm f}\,\frac{7\pi^2}{180} \simeq 4.053\,, \tag{58}$$

where the first and second terms in the right-hand side respectively correspond to the gluon and quark contributions.

Because the normalized pressure does not include direct dependence on the quark density, the values of the vector coupling constant at zero chemical potential do not affect the pressure, and the results are exactly those presented in Fig. 14.

As the quark density (or chemical potential) increases, a first-order phase transition occurs. As noted in Section 2.4, this is manifested in the appearance of three roots of the gap equation. In this case, the relation between the pressure and the chemical potential for the PNJL model and the PNJL model with $G_{\rm v}=\tilde{G}_{\rm v}(\Phi)$ is shown in Fig. 15. The mixed phase, in which quark and hadron degrees of freedom coexist, is represented by the straight line connecting two branches that form a triangle around the phase transition point. The two extreme points of this line bound a thermodynamically unstable domain in which random fluctuations can give rise to the appearance of a two-phase mixture.

The first-order phase transition corresponds to the domain of energies (temperatures) and/or densities where the derivative of pressure with respect to the quark density becomes negative. The domain boundary itself (the spinodal) is determined by setting the derivative of pressure with respect to quark density to zero. This is clear from Fig. 16, where the spinodal domain boundary is shown by a dashed line. Figure 16 also suggests that the instability region corresponds to the domain where $\partial m/\partial\mu<0$. We note that with increasing vector interaction, the instability region decreases and the first-order phase transition weakens.

3.2 Effect of meson correlations on the hadron matter equation of state

All calculations in the PNJL model presented in Sections 2 and 3.1 were carried out in the MF approximation, which enabled only the quark contribution to the pressure to be estimated. Nevertheless, it is quite possible that not only quarks but also mesons (mixed phase) can be present near the

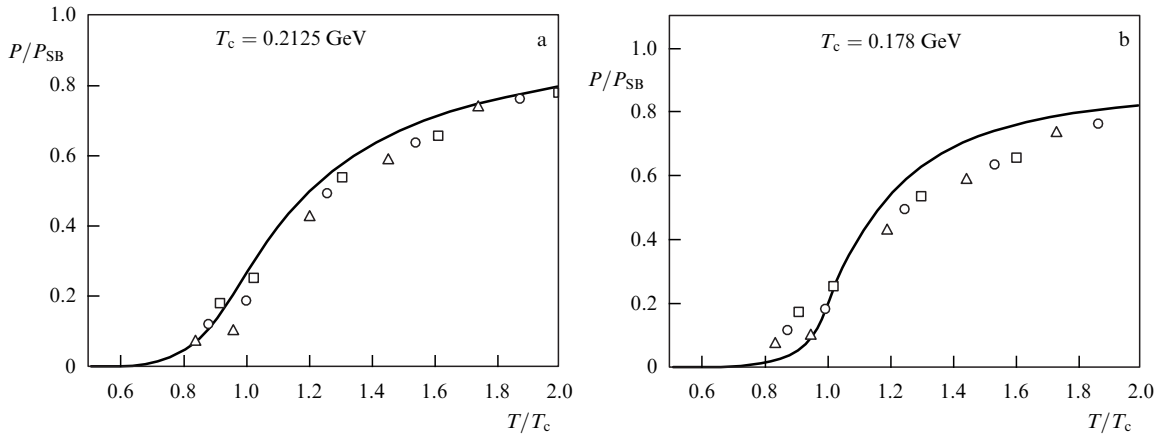

Figure 14. Normalized pressure as a function of temperature at $\mu=0$ and $G_{\rm v}=0$ for (a) the PNJL model and (b) the PNJL model with Φ-dependent coupling constants. Lattice data for $N_{\rm f}=2$ at $\mu=0$ are taken from [90]. Unfilled squares, circles, and triangles correspond to $N_t=6$ with the respective pseudoscalar-to-vector meson mass ratios $m_{\rm PS}/m_{\rm v}=0.65$, 0.70, and 0.75.

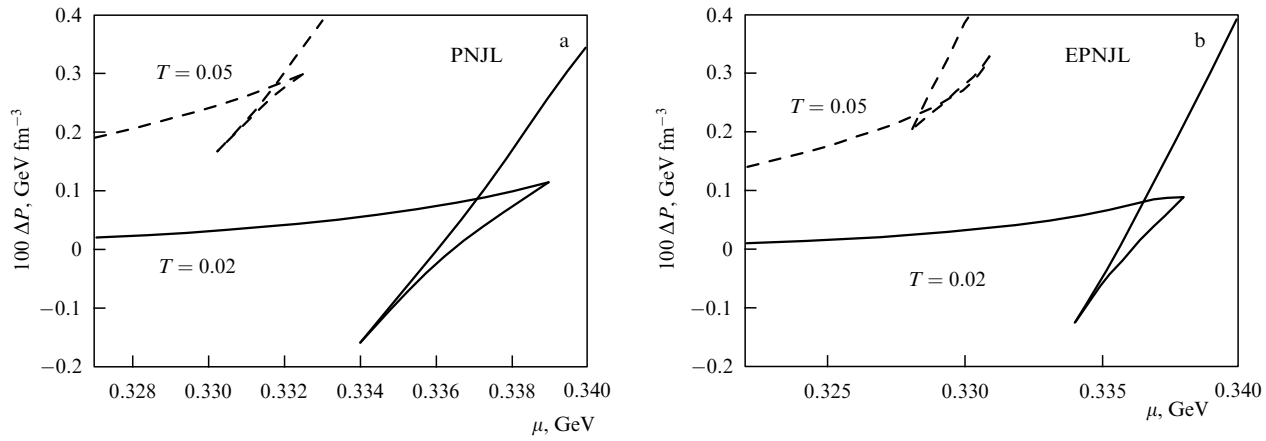

Figure 15. Pressure as a function of the chemical potential for (a) the PNJL model and (b) the PNJL model with $G_v(\Phi)$ for different temperatures.

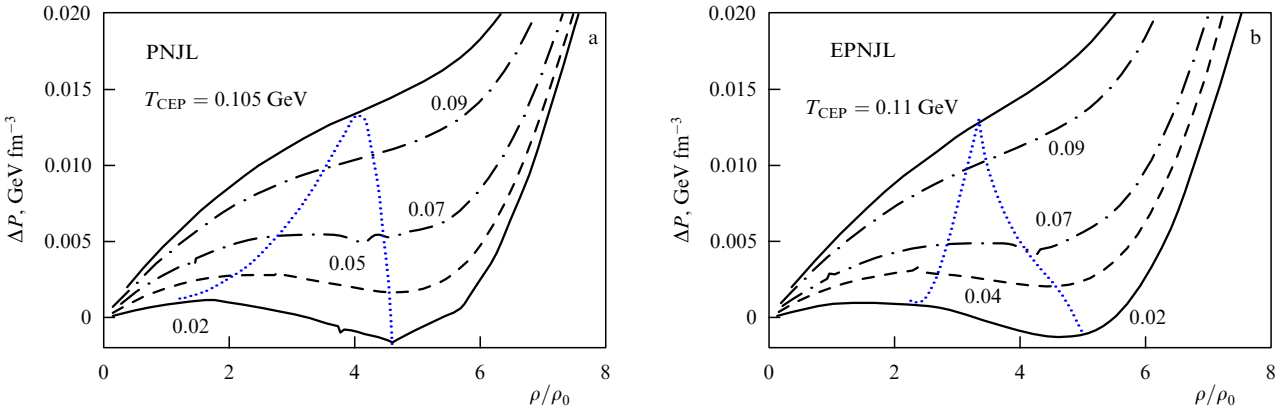

Figure 16. Pressure ΔP (solid, dashed and dashed-dotted lines) as a function of the quark density for (a) the PNJL model and (b) the PNJL model with $G_v(\Phi)$ for different temperatures indicated near the curves. The dotted curve depicts the spinodal domain boundary.

crossover boundary and contribute to the system pressure. To obtain the equation of state of a quark–hadron system [92, 93] so as to allow assessing the contributions of the bound states to the thermodynamics of the system near the phase transition, it is necessary to include the part of functional integral (50) responsible for fluctuations, which is usually ignored in the MF approximation:

$$\mathcal{Z}_{\rm FL}[T,V,\mu] = \int \mathcal{D}\sigma\mathcal{D}\pi \exp\left\{-\left(\int_0^\beta \mathrm{d}\tau \int_V \mathrm{d}^3x\, \frac{2\sigma\sigma_{\rm MF}+\sigma^2+\pi^2}{4G_{\rm s}}\right) + \mathrm{tr}\,\ln\left[1 - S_{\rm MF}[m](\sigma + \mathrm{i}\gamma_5\tau\pi)\right]\right\}. \quad (59)$$

Accounting for this term allows describing bound quark states and their effect on the thermodynamics of the system. After some transformations, integration over the external fields yields

$$\mathcal{Z}^{(2)}_{\rm FL}[T,V,\mu] = \left[\det\left(D_\sigma^{-1}\right)\right]^{-1/2}\left[\det\left(D_\pi^{-1}\right)\right]^{-3/2} \quad (60)$$

with the meson propagator

$$D_M^{-1} = \frac{1}{2G_{\rm s}} - \Pi_M(q_0,\mathbf{q})\,. \quad (61)$$

Using the identity

$$\left[\det D_M^{-1}\right]^{-n/2} = \exp\left(-\frac{N}{2}\,\mathrm{tr}\,\ln D_M^{-1}\right), \quad (62)$$

where $N = 1$ for a σ-meson and $N = 3$ for a pion, we obtain the grand thermodynamic potential

$$\Omega_{\rm FL} = \frac{1}{2}\frac{T}{V}\,\mathrm{tr}\,\ln D_\sigma^{-1} + \frac{3}{2}\frac{T}{V}\,\mathrm{tr}\,\ln D_\pi^{-1}\,. \quad (63)$$

The logarithm of the propagator can be conveniently expressed in terms of the spectral function $A_M^g(\omega,\mathbf{q})$ [94]:

$$\ln D_M^{-1} = -\int_0^{G_{\rm s}} \mathrm{d}g\,\frac{1}{2g^2}\,\frac{1}{1/(2g) - \Pi_M(q_0,\mathbf{q})} = -\int_{-\infty}^{+\infty}\frac{\mathrm{d}\omega}{2\pi}\,\frac{1}{q_0-\omega}\int_0^{G_{\rm s}}\frac{\mathrm{d}g}{2g^2}\,A_M^g(\omega,\mathbf{q})\,; \quad (64)$$

here, g is a parameter that has the meaning of some coupling constant over which integration is performed. We next analytically continue the propagator to the complex plane via a small shift $\omega \pm \mathrm{i}\eta$ from the real axis:

$$\int_0^{G_{\rm s}}\frac{\mathrm{d}g}{2g^2}\,A_M^g(\omega,\mathbf{q}) = -\mathrm{i}\int_0^{G_{\rm s}}\frac{\mathrm{d}g}{2g^2}\left(S_M^g(\omega+\mathrm{i}\eta,\mathbf{q}) - S_M^g(\omega-\mathrm{i}\eta,\mathbf{q})\right) = -\mathrm{i}\ln\left(\frac{1-2G_{\rm s}\Pi_M(\omega-\mathrm{i}\eta,\mathbf{q})}{1-2G_{\rm s}\Pi_M(\omega+\mathrm{i}\eta,\mathbf{q})}\right) = -\mathrm{i}\ln\mathcal{S}_M = 2\Phi_M\,, \quad (65)$$

where $\Phi_M(\omega, q)$ is the phase shift and $\mathcal{S}_M(\omega, \mathbf{q})$ is the scattering matrix [95]. Hence, we obtain

$$\int_0^{G_s} \frac{\mathrm{d}g}{2g^2}\, A_M^g(\omega, \mathbf{q}) = -\mathrm{i} \ln \mathcal{S}_M(\omega, \mathbf{q}) = 2\Phi_M(\omega, \mathbf{q})\,. \quad (66)$$

After substituting (66) in formulas (63) and (64), taking the trace, and integrating by parts, we arrive at the result

$$\begin{aligned}\Omega_M^{(2)}(T,\mu) &= -\frac{N_M}{2}\int \frac{\mathrm{d}^3 q}{(2\pi)^3}\int_0^{+\infty}\frac{\mathrm{d}\omega}{\pi}\,\frac{\mathrm{d}}{\mathrm{d}\omega}\\ &\times\Big(-\omega + T\ln\big\{1-\exp\big[\beta(\omega-\mu)\big]\big\}\\ &+ T\ln\big\{1-\exp\big[\beta(\omega+\mu)\big]\big\}\Big)\Phi(\omega,\mathbf{q})\\ &= -\frac{N_M}{2}\int \frac{\mathrm{d}^3 q}{(2\pi)^3}\int_0^{+\infty}\frac{\mathrm{d}\omega}{\pi}\\ &\times\Big(-\omega + T\ln\big\{1-\exp\big[\beta(\omega-\mu)\big]\big\}\\ &+ T\ln\big\{1-\exp\big[\beta(\omega+\mu)\big]\big\}\Big)\frac{\mathrm{d}\Phi_M(\omega,\mathbf{q})}{\mathrm{d}\omega}\,, \end{aligned} \quad (67)$$

where $\Phi_M(-\omega, \mathbf{q}) = -\Phi_M(\omega, \mathbf{q})$ is the scattering phase.

A further estimate of the pressure includes a physical interpretation and analytic description of the propagator $1 - 2G_s\Pi_M(\omega, \mathbf{q})$. This can be illustrated from the standpoint of the simplest assumption that the propagator has the pole approximation

$$1 - 2G_s\Pi_M(\omega, \mathbf{q}) = (\omega^2 - E_M^2)\, g_{Mqq}^2\,, \quad (68)$$

where $E_M^2 = \mathbf{q}^2 + m_M^2$ is the meson energy and m_M is the meson mass. Then

$$\frac{\mathrm{d}}{\mathrm{d}\omega}\ln\frac{1-2G_s\Pi_M(\omega-\mathrm{i}\eta,\mathbf{q})}{1-2G_s\Pi_M(\omega+\mathrm{i}\eta,\mathbf{q})} = -2\pi\mathrm{i}\delta(\omega - E_M)\,, \quad (69)$$

and the thermodynamic potential is

$$\begin{aligned}\Omega_M = \frac{N_M}{2}\int\frac{\mathrm{d}^3 q}{q}\,\Big(&E_M + T\ln\big\{1-\exp\big[-\beta(E_M-\mu)\big]\big\}\\ &+ T\ln\big\{1-\exp\big[-\beta(E_M+\mu)\big]\big\}\Big)\,. \end{aligned} \quad (70)$$

Such a potential corresponds to a system of noninteracting mesons [96].

By combining the contribution from bound states described by the delta function and the contribution from scattering states ($\mathrm{d}\Phi_M/\mathrm{d}\omega$), it is possible to obtain a generalized Bethe–Uhlenbeck equation. Masses of the bound states and the scattering phase shift in the corresponding channel depend on the scattering medium. For example, chiral symmetry restoration sharply reduces the quark mass to a current value in the phase transition domain. The pions then become resonance states that can be described by the complex pole $q_0 = m_M - \mathrm{i}\Gamma_M/2$, where Γ_M is the resonance state width. By ignoring the medium effects, it is possible to calculate the effect of the meson resonance state broadening. For this, a spectral Breit–Wigner (BW) function is introduced:

$$\frac{\mathrm{d}\Phi_R(\omega,T)}{\mathrm{d}s} = A_R(\omega,T) = a_R\,\frac{m_M\Gamma_M}{(\omega-m_M)^2+(m_M\Gamma_M)^2}\,, \quad (71)$$

where a_R is the normalization factor determined from the standard normalization condition:

$$\int_{-q^2}^{+\infty}\mathrm{d}\omega\, A_R = a_R\int_{-q^2}^{+\infty}\mathrm{d}\omega\,\frac{m_M\Gamma_M}{(\omega-m_M)^2+(m_M\Gamma_M)^2} = 1\,, \quad (72)$$

whence

$$a_R = \frac{\pi}{\pi/2 + \arctan\big[(\mathbf{q}^2+m_M^2)/(m_M\Gamma_M)\big]}\,. \quad (73)$$

The width of mesons is virtually zero for temperatures below the Mott temperature T_{Mott} and becomes finite for $T > T_{\mathrm{Mott}}$, describing the spectral broadening of the resonance states. To determine Γ_M, it is usually assumed that the polarization function can be analytically continued into the complex plane (as was similarly done in (65)): $m_M \pm \mathrm{i}\epsilon$. From (25) and (26), we then obtain the system of equations

$$\mathrm{Re}\, P_M = -\frac{1/(4G_sN_cN_f) - 2I_1}{\big|I_2(m_M+\mathrm{i}\epsilon)\big|^2}\,\mathrm{Re}\, I_2(m_M+\mathrm{i}\epsilon)\,, \quad (74)$$

$$\mathrm{Im}\, P_M = -\frac{1/(4G_sN_cN_f) - 2I_1}{\big|I_2(m_M+\mathrm{i}\epsilon)\big|^2}\,\mathrm{Im}\, I_2(m_M+\mathrm{i}\epsilon)\,, \quad (75)$$

where $\mathrm{Re}\, P_M = m_\pi^2 - \Gamma_\pi^2/4$ for a pion and $\mathrm{Re}\, P_M = m_\sigma^2 - 4m^2 - \Gamma_\sigma^2/4$ for a σ-meson, and $\mathrm{Im}\, P_M = m_M\Gamma_M$ for both mesons.

The temperature behavior of the meson masses and widths is presented in Fig. 17. The figure shows that the σ-meson has a nonzero width even at temperatures below T_{Mott}, but because this value is close to zero, a σ-meson is considered a bound state. For $T > T_{\mathrm{Mott}}$, the meson masses, as well as their widths, rapidly become identical. This confirms the chiral symmetry restoration: a σ-meson and a pion become chiral partners.

If all necessary quantities are known, their substitution in (67) allows calculating the pressure. Figure 18b shows both the pressure of mesons for a noninteracting meson gas and the pressure with spectral broadening taken into account. It is clearly seen that at temperatures $T \geqslant T_{\mathrm{Mott}}$, the pressure of the mesons decreases, which is related to the melting of bound states. A comparison of the meson pressure and the quark pressure calculated in the MF approximation is presented in Fig. 18a.

It was shown in [62, 95] that in the NJL and PNJL models, the Levinson theorem holds for pions, relating the scattering phase shift to the number of bound states in the system. In the integral form, this relation can be expressed as

$$\int_{4m^2}^{+\infty}\mathrm{d}\omega\,\frac{\mathrm{d}\Phi_M}{\mathrm{d}\omega} = n\pi\,, \quad (76)$$

where n is the number of bound states in the system. As shown in [62], to satisfy the Levinson lemma, the phase shift Φ_M taken in form (71) must be split into parts: the phase shift corresponding to quark–quark and quark–antiquark scatterings (the background phase shift ϕ_{sc}), and the phase shift caused by correlations of mesons (ϕ_R). The phase shift Φ_M and the degree of realization of this theorem in the PNJL model for pions ($n = 1$) are shown in Fig. 19. Figures 19a, b show the phase shift due to quark–quark scatterings (ϕ_{sc}) and the phase shift due to meson correlations (ϕ_R). As seen from Fig. 19a, at $T < T_{\mathrm{Mott}}$, a pion is a bound state; therefore, the

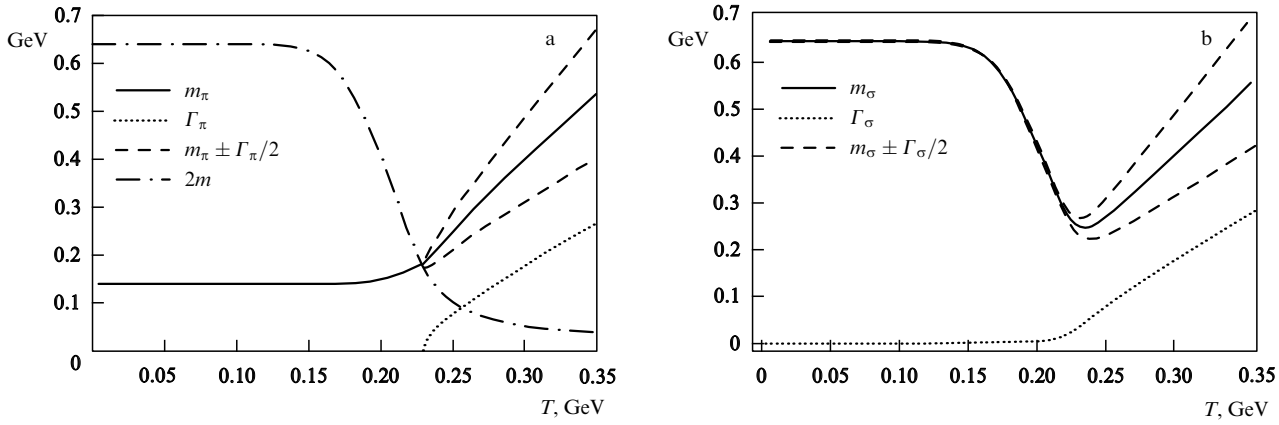

Figure 17. The mass, width, and double mass ($2m$) of the quark for (a) a π-meson and (b) a σ-meson as a function of temperature in the PNJL model at $\mu = 0$.

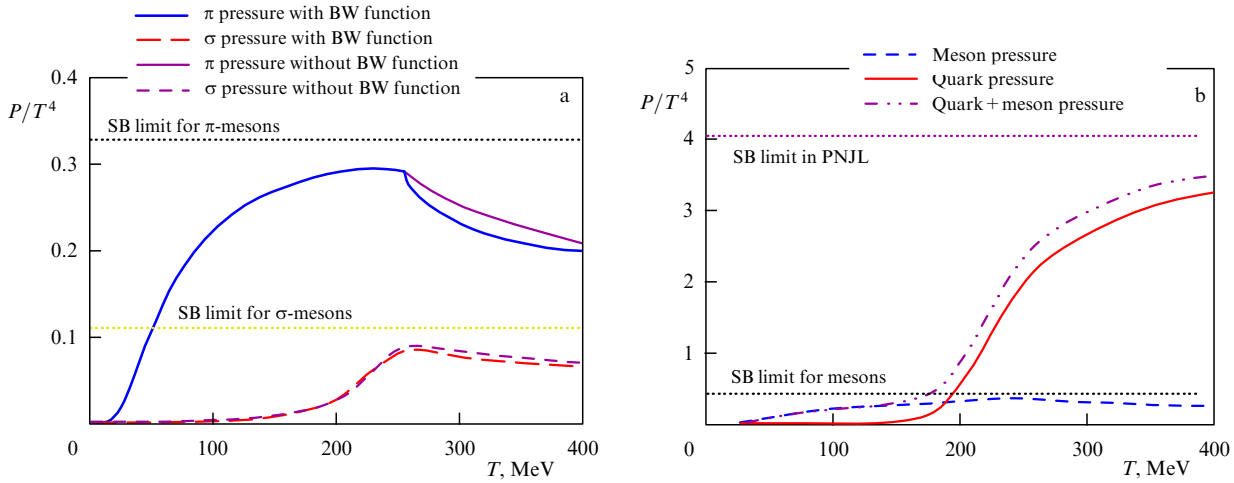

Figure 18. (a) Meson pressure with and without taking spectral broadening and scattering into account and (b) a comparison of the meson pressure and the quark system pressure in the MF approximation in the PNJL model at $\mu = 0$. The horizontal dotted lines show the Stephan–Boltzmann (SB) limit.

phase shift demonstrates a jump from 0 to π. For $T > T_{\text{Mott}}$, a pion becomes a resonance state, and the phase shift in the energy range from 0 to $\sqrt{s} = m_\pi$ gradually increases from 0 to π. At higher temperatures, the phase shift ceases to reach π, which suggests the absence of bound states in the system. The background phase shift ϕ_{sc} shown in Fig. 19b is due to quark–quark scatterings with the intermediate formation of π- and σ-mesons, and at low temperatures it has the threshold $s = 2m$. Clearly, with increasing the temperature, the background phase shift stops changing. Figure 19c presents the total phase shift.

4. Conclusion

The PNJL model arose from the attempt to unify the properties of chiral models with confinement. The PNJL model is one of a few enabling a description of both the chiral phase transition and the confinement–deconfinement phase transition.

Confinement in the PNJL model is determined by the effective potential, which is in turn found by approximating lattice QCD data in the absence of dynamic quarks. In this connection, the PNJL model is in good agreement with lattice QCD data at finite temperatures. To study the properties of nuclear matter at finite chemical potentials, lattice QCD calculations increasingly use an imaginary chemical potential; these results can then be extrapolated into the domain of finite real chemical potentials. But it turns out that such a straightforward extrapolation into the region of real chemical potentials gives reasonable results only for low values of μ/T [43–45]. This problem can be solved if there is an effective model capable of correctly estimating the partition function for both real and imaginary chemical potentials, i.e., capable of reproducing the lattice QCD data in the imaginary chemical potential domain [58]. The PNJL model can be such a model. It was shown in [58, 97, 98] that the PNJL model also satisfies the extended Z_3-symmetry [$\Omega(\Theta) = \Omega(\Theta + 2\pi k/N)$ for the $Z(N)$-symmetry] [76] if a modified function of the Polyakov-loop field is introduced: $\Psi = \exp(\mathrm{i}\Theta)\Phi$ and $\bar{\Psi} = \exp(-\mathrm{i}\Theta)\bar{\Phi}$. This assumption stimulated searches for the CEP [99–103].

A limitation of the PNJL model, as well as the NJL model, is the need of regularization. The three-dimensional momentum cutoff restricts the applicability of the model to the region $|\mathbf{p}| < \Lambda$, which, for example, precludes perturbative QCD phenomena to be studied. A nonlocal NJL model with a Polyakov loop is free from these shortcomings. The nonlocality of the four-quark interaction gives rise to a momentum

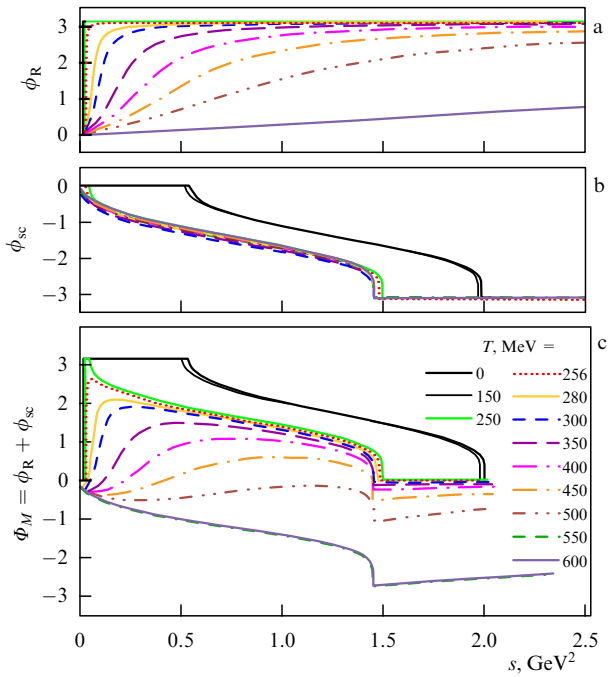

Figure 19. Phase shift.

dependence of the dynamic mass of quarks. The use of the momentum-dependent dynamic quark mass enables a direct comparison of the model results with lattice QCD calculations [104] and a decrease in the critical temperature and density for the CEP on the phase diagram. It was shown in [36, 38] that the CEP location depends on the model parameters. As shown in [61], the CEP location on the phase diagram is highly sensitive to changes in the parameters of the nonlocal interaction form factors and to taking the vector interaction into account. For some model parameters, the CEP disappears on the phase diagram.

Thus, the PNJL model can be used to solve a broad range of problems related to the thermodynamic properties of dense hot nuclear matter that are relevant in ion collisions and under the conditions existing in neutron star cores. The PNJL model is also used for calculations related to the CP-invariance violation in strong interactions as a consequence of the chiral anomaly effect on the topological structure of the QCD vacuum in strong magnetic fields generated in heavy-ion collisions [105, 106]. However, so far, the results obtained in the NJL and PNJL models disagree with lattice QCD calculations [107].

In addition, the PNJL model enables studies of quark scattering on quarks and light mesons [108, 109], as well as the processes of decay and scattering of light mesons at finite temperatures [110–112].

Acknowledgments

The authors thank D Blaschke for collaboration and the invaluable contribution to this paper. The work of Yu L K is supported by the Russian Foundation for Basic Research grant No. 13-01-00060a.

References

1. Greiner W, Schäfer A *Quantum Chromodynamics* (Berlin: Springer-Verlag, 1994)
2. Ejiri S *Nucl. Phys. B Proc. Suppl.* **94** 19 (2001)
3. Bazavov A et al. *Phys. Rev. D* **85** 054503 (2012); arXiv:1111.1710
4. Wu L-K, Luo X-Q, Chen H-S *Phys. Rev. D* **76** 034505 (2007)
5. Nambu Y, Jona-Lasinio G *Phys. Rev.* **122** 345 (1961)
6. Nambu Y, Jona-Lasinio G *Phys. Rev.* **124** 246 (1961)
7. Gell-Mann M, Lévy M *Nuovo Cimento* **16** 705 (1960)
8. Eguchi T *Phys. Rev. D* **14** 2755 (1976)
9. Kikkawa K *Prog. Theor. Phys.* **56** 947 (1976)
10. Volkov M K, Ebert D *Sov. J. Nucl. Phys.* **36** 736 (1982); *Yad. Fiz.* **36** 1265 (1982)
11. Ebert D, Volkov M K *Z. Phyz. C* **16** 205 (1983)
12. Volkov M K *Ann. Physics* **157** 282 (1984)
13. Volkov M K *Sov. J. Part. Nucl.* **17** 186 (1986); *Fiz. Elem. Chastits At. Yadra* **17** 433 (1986)
14. Hatsuda T, Kunihiro T *Phys. Rev. Lett.* **55** 158 (1985)
15. Hatsuda T, Kunihiro T *Phys. Lett. B* **185** 304 (1987)
16. Kunihiro T *Phys. Lett. B* **219** 363 (1989)
17. Klevansky S P *Rev. Mod. Phys.* **64** 649 (1992)
18. Bernard V, Meissner U-G, Zahed I *Phys. Rev. D* **36** 819 (1987)
19. Bernard V, Meissner U-G, Zahed I *Phys. Rev. Lett.* **59** 966 (1987)
20. Christov C V, Ruiz-Arriola E, Goeke K *Acta Phys. Polon. B* **22** 187 (1991)
21. Hüfner J, Klevansky S P, Zhuang P *Acta Phys. Polon. B* **25** 85 (1994)
22. Kalinovsky Yu L, Friesen A V *Phys. Part. Nucl. Lett.* **12** 737 (2015); *Pis'ma Fiz. Elem. Chastits At. Yadra* **12** 1143 (2015)
23. Efimov G V, Ivanov M A *Sov. J. Part. Nucl.* **20** 479 (1989); *Pis'ma Fiz. Elem. Chastits At. Yadra* **20** 1129 (1989)
24. Andrianov A A, Espriu D, Tarrach R *Nucl. Phys. B* **533** 429 (1998)
25. Celenza L S et al. *Phys. Rev. C* **60** 025202 (1999); *Phys. Rev. C* **60** 039901 (1999) Erratum
26. Dyakonov D I, Petrov V Yu *Nucl. Phys. B* **272** 457 (1986)
27. Buballa M, Krewald S *Phys. Lett. B* **294** 19 (1992)
28. Anikin I V, Dorokhov A E, Tomio L *Phys. Part. Nucl.* **31** 509 (2000); *Fiz. Elem. Chastits At. Yadra* **31** 1023 (2000)
29. Polyakov A M *Phys. Lett. B* **72** 477 (1978)
30. Meisinger P N, Ogilvie M C *Phys. Lett. B* **379** 163 (1996)
31. Meisinger P N, Miller T R, Ogilvie M C *Phys. Rev. D* **65** 034009 (2002)
32. Mócsy A, Sannino F, Tuominen K *Phys. Rev. Lett.* **92** 182302 (2004)
33. Fukushima K *Phys. Lett. B* **591** 277 (2004)
34. Ratti C, Thaler M A, Weise W *Phys. Rev. D* **73** 014019 (2006)
35. Hansen H et al. *Phys. Rev. D* **75** 065004 (2007)
36. Rößner S, Ratti C, Weise W *Phys. Rev. D* **75** 034007 (2007)
37. Costa P et al. *Phys. Rev. D* **81** 016007 (2010)
38. Fukushima K *Phys. Rev. D* **77** 114028 (2008)
39. Lugones G et al. *Phys. Rev. D* **81** 085012 (2010)
40. Lenzi C H et al. *Phys. Rev. C* **82** 015809 (2010)
41. Dexheimer V et al. *Phys. Rev. C* **87** 015804 (2013)
42. Borsányi S et al. *JHEP* (09) 073 (2010)
43. de Forcrand P, Philipsen O *Nucl. Phys. B* **642** 290 (2002)
44. D'Elia M, Lombardo M-P *Phys. Rev. D* **67** 014505 (2003)
45. D'Elia M, Di Renzo F, Lombardo M-P *Phys. Rev. D* **76** 114509 (2007)
46. Kogut J B, Sinclair D K *Phys. Rev. D* **70** 094501 (2004)
47. Cea P et al. *Phys. Rev. D* **80** 034501 (2009)
48. Sakai Y et al. *Phys. Rev. D* **82** 076003 (2010)
49. Sakai Y et al. *J. Phys. G* **39** 035004 (2012); arXiv:1104.2394
50. Ruivo M C, Costa P, de Sousa C A *Phys. Rev. D* **86** 116007 (2012)
51. Sugano J et al. *Phys. Rev. D* **90** 037901 (2014)
52. Friesen A V, Kalinovsky Yu L, Toneev V D *Int. J. Mod. Phys. A* **30** 1550089 (2015)
53. Vogl U, Weise W *Prog. Part. Nucl. Phys.* **27** 195 (1991)
54. Buballa M *Phys. Rep.* **407** 205 (2005)
55. Lourenco O *Phys. Rev. D* **85** 097504 (2012)
56. Dutra M et al. *Phys. Rev. D* **88** 114013 (2013)
57. Fukushima K *Phys. Rev. D* **78** 114019 (2008)
58. Sakai Y et al. *Phys. Rev. D* **78** 076007 (2008)
59. Carignano S, Nickel D, Buballa M *Phys. Rev. D* **82** 054009 (2010)
60. Steinheimer J, Schramm S *Phys. Lett. B* **696** 257 (2011)
61. Contrera G A, Grunfeld A G, Blaschke D B *Phys. Part. Nucl. Lett.* **11** 342 (2014); *Pis'ma Fiz. Elem. Chastits At. Yadra* **11** 544 (2014)
62. Wergieluk A et al. *Phys. Part. Nucl. Lett.* **10** 660 (2013); *Pis'ma Fiz. Elem. Chastits At. Yadra* **10** 1084 (2013)
63. Simonov Yu A *Phys. Usp.* **39** 313 (1996); *Usp. Fiz. Nauk* **166** 337 (1996)

64. Pisarski R D, in *QCD Perspectives on Hot and Dense Matter, Proc. of the Cargese Summer School, 6 – 18 August 2001, Cargese, France* (NATO Science Series, II, Vol. 87, Eds J P Blaizot, E Iancu) (Dordrecht: Kluwer, 2002) p. 353; hep-ph/0203271
65. Pisarski R D *Phys. Rev. D* **62** 111501(R) (2000)
66. Boyd G et al. *Nucl. Phys. B* **469** 419 (1996)
67. Rößner S et al. *Nucl. Phys. A* **814** 118 (2008)
68. Dexheimer V A, Schramm S *Nucl. Phys. A* **827** 579c (2009)
69. Dexheimer V A, Schramm S *Phys. Rev. C* **81** 045201 (2010)
70. Panero M *Phys. Rev. Lett.* **103** 232001 (2009)
71. Meisinger P N, Ogilvie M C, Miller T R *Phys. Lett. B* **585** 149 (2004)
72. Karsch F, Laermann E, Peikert A *Phys. Lett. B* **478** 447 (2000)
73. Karsch F *Nucl. Phys. A* **698** 199 (2002)
74. Ratti C, Rößner S, Weise W *Phys. Lett. B* **649** 57 (2007); hep-ph/0701091
75. Kondo K-I *Phys. Rev. D* **82** 065024 (2010)
76. Roberge A, Weiss N *Nucl. Phys. B* **275** 734 (1986)
77. Dutra M et al. *Phys. Rev. D* **88** 114013 (2013)
78. Sugano J et al. *Phys. Rev. D* **90** 037901 (2014)
79. Endrődi G et al. *JHEP* **2011** (4) 1 (2011)
80. Kaczmarek O et al. *Phys. Rev. D* **83** 014504 (2011)
81. Bonati C et al. *Phys. Rev. D* **90** 114025 (2014); arXiv:1410.5758
82. Braguta V V et al. *JETP Lett.* **101** 732 (2015); *Pis'ma Zh. Eksp. Teor. Fiz.* **101** 827 (2015)
83. Cea P, Cosmai L, Papa A *Phys. Rev. D* **89** 074512 (2014)
84. Masayuki A, Koichi Y *Nucl. Phys. A* **504** 668 (1989)
85. Scavenius O et al. *Phys. Rev. C* **64** 045202 (2001); nucl-th/0007030
86. Ejiri S et al. *Theor. Phys. Suppl.* **153** 118 (2003)
87. Gavai R V, Gupta S *Phys. Rev. D* **71** 114014 (2005)
88. Fodor Z, Katz S D *JHEP* (03) 014 (2002)
89. Fodor Z, Katz S D *JHEP* (04) 050 (2004)
90. Ali Khan A et al. (CP-PACS Collab.) *Phys. Rev. D* **64** 074510 (2001)
91. Friesen A V, Kalinovsky Yu L, Toneev V D *Int. J. Mod. Phys. A* **27** 1250013 (2012)
92. Uhlenbeck G E, Beth E *Physica* **3** 729 (1936)
93. Beth E, Uhlenbeck G E *Physica* **4** 915 (1937)
94. Abuki H *Nucl. Phys. A* **791** 117 (2007)
95. Hufner J et al. *Ann. Physics* **234** 225 (1994)
96. Kapusta J I *Finite-Temperature Field Theory* (Cambridge: Cambridge Univ. Press, 1989)
97. Sakai Y et al. *Phys. Rev. D* **77** 051901 (2008)
98. Sakai Y et al. *Phys. Rev. D* **78** 036001 (2008)
99. Pagura V, Gómez Dumm D, Scoccola N N *Phys. Lett. B* **707** 76 (2012); arXiv:1105.1739
100. Kouno H et al. *Phys. Rev. D* **83** 076009 (2011)
101. Kashiwa K et al. *Phys. Rev. D* **79** 076008 (2009)
102. Scheffler D, Buballa M, Wambach J, *FAIR Workshop and XXVIII Max Born Symposium "Three Days on Quarkyonic Island", Wrocaw, Poland, May 19 – 21, 2011*; arXiv:1111.3839
103. Morita K et al., in *Three Days on Quarkyonic Island, HIC for FAIR Workshop and XXVIII Max Born Symp. Satellite Meeting for Quark Matter 2011, Wroclaw, Poland, 19 – 21 May 2011*; arXiv:1111.3446
104. Hell T et al. *Phys. Rev. D* **79** 014022 (2009)
105. Chatterjee B, Mishra H, Mishra A *Phys. Rev. D* **91** 034031 (2015)
106. Fukushima K, Ruggieri M, Gatto R *Phys. Rev. D* **81** 114031 (2010)
107. Braguta V V et al. *JHEP* **2015** (6) 094 (2015)
108. Rehberg P, Klevansky S P, Hüfner J *Phys. Rev. C* **53** 410 (1996)
109. Friesen A V, Kalinovsky Yu L, Toneev V D *Nucl. Phys. A* **923** 1 (2014)
110. Friesen A V, Kalinovsky Yu L, Toneev V D *Phys. Part. Nucl. Lett.* **9** 1 (2012); *Pis'ma Fiz. Elem. Chastits At. Yadra* **9** 8 (2012)
111. Zhuang P-F, Yang Z-W *Chinese Phys. Lett.* **18** 344 (2001); nucl-th/0008041
112. Fu W, Liu Y *Phys. Rev. D* **79** 074011 (2009)